Ibada, Nigeria) populations. These SNPs were in strong LD in JPT and CEU populations, although relatively low LD was predicted in the YRI population [14,16], suggesting that any of the SNPs located in this region could be responsible for treatment response. Because of the strong LD, tests for independence among these variants were not able to reveal which of these SNPs is uniquely responsible for the association with virological response (VR) or non-virological response (NVR). The identification of the primary genetic variant located in the LD block remained critical, although the risk haplotype tended to influence the expression levels or activity of *IL-28B* [13,14]. In this study, we sought to determine the primary SNP affecting IL-28B expression and/or its function by focusing on the proximal regulatory region of *IL-28B*.

IL-28B was discovered as a member of the IFN-λ family by Sheppard et al. and Kotenko et al. [1,2]. They discovered this family, *IL-29*, *IL-28A*, and *IL-28B* and the specific receptor, *IL-28RI*, by applying individual computational techniques to the draft human genome. However, the start codon of IFN-λ differs between the reports, with an additional 12 nucleotides at the N-terminus in all IFN-λs reported by Sheppard et al. (Fig. S1). The sequence similarity between these ORFs is approximately 96.7% and, especially, there is a high degree of identity between *IL-28A* and *IL-28B* cDNA (approximately 98%). Figure 1A shows the locations of *IL-28A/B* gene, the significant SNPs around *IL-28B* related to anti-HCV therapy reported in previous studies [12,13,14], and $(TA)_n$ repeats in the regulatory region of *IL-28A* and *B*. The SNPs information assessed in this study is summarized in Table 1 and the locations of the SNPs are shown in the schematic of the *IL-28B* gene (Fig. 1B). The reference sequences of *IL-28A* or *IL-28B* cDNA, registered in NCBI CCDS, are composed of 6 exons and 5 exons, respectively (Fig. 1B). Because high sequence similarity was observed between *IL-28A* and *IL-28B* from CpG to the region downstream of 3′-UTR (Fig. S2), the genes were almost completely identical around transcription start site (TSS) (>99%). Then, we determined the likely gene structure using a complete cDNA cloning method because a similar transcriptional mechanism was expected for *IL-28A* and *IL-28B*.

Materials and Methods

Genome samples

Genome samples were obtained from 20 healthy volunteers (HV). Peripheral blood mononuclear cells (PBMC) collected from HV were isolated using the BD Vacutainer CPT Method (BD Biosciences). Genomic DNAs were extracted by standard methods. SNPs were selected from the database at GWAS database (https://gwas.lifesciencedb.jp/cgi-bin/gwasdb/gwas_top.cgi). Written informed consent was provided by all participants in the genotyping study following procedures approved by the Ethical Committee at Nagoya City University.

Cell lines

Human hepatocellular carcinoma cell lines, HepG2 and HuH7, human hepatocyte cell lines, HuSE2 (kindly provided by Dr. Hijikata in Kyoto University), and the human cervical cancer cell line, HeLa (obtained from The American Type Culture Collection), were cultured in Dulbecco's modified Eagle's medium supplemented with 10% (v/v) fetal bovine serum, 100 U ml^{-1} penicillin and 100 mg ml^{-1} streptomycin. Human leukemia virus type 1 transformed cell line, MT-2 (a gift from Dr. Ueda in Nagoya City University), Burkitt lymphoma cell line, Raji, and human T cell leukemia cell line, Jurkat (obtained from The American Type Culture Collection), were cultured in RPMI 1640 medium supplemented with 10% (v/v) fetal bovine serum, 100 U ml^{-1} penicillin and 100 mg ml^{-1} streptomycin. All incubations were performed at 37°C in a 5% CO_2 gassed incubator. Recombinant human IFN-λ2 and -3 were purchased from R&D Systems (Abingdon, UK). Natural human IFN-α was

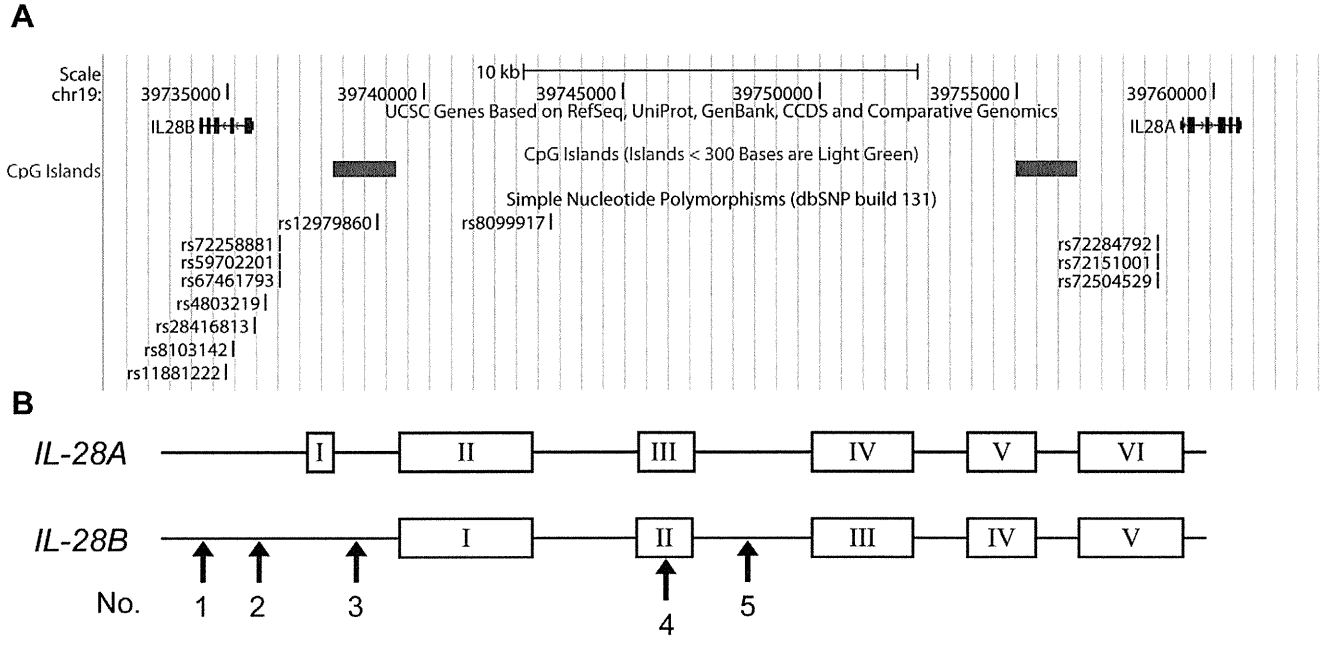

Figure 1. The position of significant SNPs and *IL-28A/B* in chromosome 19, retrieved from the database. (A) The *IL-28A/B* genes located in chromosome 19q13 are described in the genome map of the UCSC genome browser. The significant proximal SNPs around *IL-28B* associated with response to PEG-IFN/RBV therapy are shown in the map [14]. SNPs of $(TA)_n$ variation at the regulatory region of *IL-28A* are displayed in the position corresponding to that of *IL-28B*, which is not associated with anti-HCV therapy. (B) The schematic of *IL-28A/B* gene structure is described based NCBI CCDS data. Arrows show five significant SNPs examined in this study (see Table 1).
doi:10.1371/journal.pone.0026620.g001

Table 1. Significant SNPs around *IL-28B*.

Feature	rs ID	Allele 1/2*[1]	Minus strand*[2]	Location	No.
DIP*[3]	rs72258881*[4]	ATAT/-	TATA/-	Regulatory	1
Substitution	rs4803219	C/T	G/A	Regulatory	2
	rs28416813	C/G	G/C	Intron	3
	rs8103142	T/C	A/G	Nonsynonymous	4
	rs11881222	A/G	T/C	Intron	5

*[1]These data were derived from dbSNP. Allele 2 is the risk allele of HCV therapy reported by Tanaka *et al.*, except for rs72258881.
*[2]Complementary nucleotides are shown because *IL-28B* is coded on the minus strand.
*[3]DIP: deletion/insertion polymorphism.
*[4]The ID represents rs72258881, rs59702201, and rs67461793 because these three are located in the same genomic region, the TA repeat.
doi:10.1371/journal.pone.0026620.t001

purchased from Hayashibara co. ltd. (Okayama, Japan). The mRNA expression levels of receptors stimulated in this study were confirmed by PCR using gene specific primer (Table S1 and Fig. S3),

Plasmid Construction

As a T/G heterozygote genome of rs8099917 with a strong LD was used as the PCR template, amplicons from the major and minor alleles were obtained for the assay described below. PCR was carried out to amplify the fragment from −858 nt of the ATG site to TGA of *IL-28B*, and the products were inserted into pcDNA3.1/Hyg (pcDNA/MA or mi) or pcDNA3.1/Hyg vector deleting CMV promoter (pdCMV/MA or mi). A FLAG sequence was conjugated to 6th exon, removing the stop codon, for real time PCR analysis. The promoter region from nucleotide position −858 to +30 of *IL-28B* was amplified using pdCMV/MA or mi vector and inserted into pGL4 vector for the luciferase assay. A vector with an antisense insert was prepared as a control. For expression constructs, the wild type (WT) plasmids, pcDNA3.1/wild expressing human IL-28B, and pcDNA3.1/ns-mut expressing human IL-28B harboring a K^{74}R mutation, were generated using pcDNA3.1/V5-His-TOPO® (Invitrogen, San Diego, CA) and were used in the subsequent transfections. In addition, pcDNA3.1/AS expressing antisense strand of IL-28B was constructed as a control. We also obtained a pISRE-luc plasmid (provided by Sakamoto N., Tokyo Medical Dental University, Tokyo, Japan). The pGL4.74 vector encoding Renilla Luciferase was purchased from Promega (Madison, WI). These primer sequences are available on request. The above expression vectors were modified for the analysis of splicing function by introducing two intron SNPs (rs28416813 and rs11881222) (Table 1), which were pcDNA/WT, d-iSNPs.

Transient transfections

Transient transfections of HeLa, Jurkat, Raji, HuH7, HepG2, or HuSE2 (hepatocellular carcinomas cell line) cells were carried out using FuGene HD (Roche) or the Cell Line Nucleofector kit (Amaxa Biosystems) according to the manufacturers' protocols. Briefly, Cells (2×10^5) were seeded into a 6 well plate and transfected with for FuGene HD. For the electroporation method, cells (1.0×10^6) were collected and resuspended in Nucleofector solution V for each individual transfection sample.

5′-, 3′-RACE based on full-length cDNA cloning

Total RNA was prepared from cell lines stimulated with lipopolysaccharide (LPS) (0127:B8, Sigma-Aldrich) for 4 hours after 100 U/mL of IFN-α for 16 hours by following previous paper [17]. A GeneRacer Kit (Invitrogen Life Technologies) was used to obtain the complete cDNA sequence of *IL-28A/B* following manufacturer's instructions. Briefly, the GeneRacer RNA Oligo was ligated to the 5′ end specifically of full-length mRNA within the total RNA mixture. This ligated mRNA was then converted to cDNA using reverse transcriptase (RT) and the GeneRacer Oligo dT Primer. Next, this cDNA was used for PCR using the oligonucleotides of GeneRacer 5′ Primer and P1 primer which hybridized to the coding strand of the *IL28A/B* (Table S1). The resulting PCR products were then used for a second round of PCR using the oligonucleotides GeneRacer 5′ Nested Primer, which represents the DNA equivalent of the 3′ end of the GeneRacer RNA Oligo, and P2, which hybridizes to the coding strand of the *IL-28A/B* 5′ to the P1 hybridization site. For 3′ RACE, the cDNA was subjected to the polymerase chain reaction (PCR) to amplify the 3′ end using a forward gene-specific primer P3 designed from *IL-28A/B* and the GeneRacer 3′ primer provided with the kit. Nested PCR, using the same gene-specific primer and GeneRacer 3′ nested primer, was performed. The PCR product of 5′ and 3′ RACE was cloned into pCR4-TOPO TA vector according to the manufacturer's instructions (Invitrogen). Ten clones were isolated and subjected to automated sequencing (ABI3100, ABI) in our core facility.

Protein expression and purification

Recombinant IL-28B and its mutant were produced by transfecting Free-Style™ 293-F cells (purchased from Invitrogen, Carlsbad, CA) with the expression plasmid, which was grown in 5000 ml of FreeStyle 293 Expression Medium, following the manufacturer's recommendations (Invitrogen, Carlsbad, CA). Cultures were maintained at >90% viability on a shaker plate (Titer Plate Shaker; Lab-Line Instruments, Melrose Park, NJ) moving at 125 rpm in a 37°C incubator with 8% CO_2 and subculturing at a 1:10 ratio upon reaching a density of 2×10^6 cells per ml. Cell density and viability were evaluated with a hemocytometer using 0.4% trypan blue staining. After 96 h, the transfected cell culture was harvested. The supernatant containing the secreted recombinant protein was centrifuged (100×g, 15 min), frozen, and stored at −30°C until use. The 293-F cells supernatant containing the recombinant protein was loaded onto a Ni^{2+} column (Amersham Biosciences) following the manufacturer's directions. Fractions were eluted with 80, 100, 250, and 1000 mM imidazole (in 50 mM Tris, 300 mM NaCl, pH 8.0), and the fraction eluted at 250 mM was pooled and concentrated in an Amicon (10 kDa molecular weight cutoff) to 1 ml (Amersham Biosciences).

Western blot analyses

Purified recombinant protein was loaded onto 12% sodium dodecyl sulfate gels. Proteins were detected with goat anti-IL28 (1:2000) polyclonal antibody (Santa Cruz Biotechnology, Santa Cruz, CA) and the secondary antibody. Proteins were visualized using ECL Plus Western blotting detection reagents (GE Healthcare) and a LuminoImager (LAS-3000; Fujifilm). The band densities were analyzed with the Multi Gauge software (version 3.1; Fujifilm).

IL-28A/B promoter genotyping

Germ-line DNA was extracted from PBMC according to standard methods [14]. Twenty HV samples were genotyped for the dinucleotide insertion/deletion (indel) present in the promoter region of *IL-28A* or *B*, as described below. Twenty ng of genomic DNA were subjected to PCR analysis in 50 µl aliquots containing

A

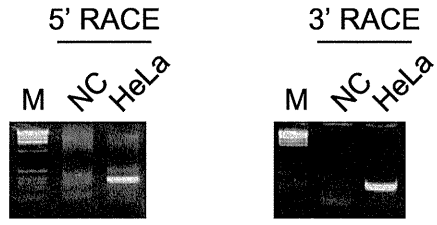

B

```
IL-28A     1 ------------------------------------------------------------     1
IL-28B     1 ------------------------------------------------------------     1
5RACE-A    1 GAATTACATCCCAGACAGAGCTCAAAACTGACAGAAAGAGTCAAAGCCAGGACACAGTCT    60
5RACE-B    1 GAATTACATCCCAGACAGAGCTCAAAACTGACAGAAAGAGTCAAAGCCAGGACACAGTCT    60

IL-28A     1 ------------------------------------------------------------     1
IL-28B     1 ------------------------------------------------------------     1
5RACE-A   61 GAGATCCAGAAGAGGGGACTGAAAAGAACAGAGACTCCAGACAAGACCCAAACAGACCCT   120
5RACE-B   61 GAGATCCAGAAGAGGGGACTGAAAAGAACAGAGACTCCAGACAAGACCCAAACAGACCCT   120

IL-28A     1 ----------------------------------------------------ATGAAACTA     9
IL-28B     1 ------------------------------------------------------------     1
5RACE-A  121 GGGTGACAGCCTCAGAGTGTTTCTTCTGCTGACAAAGACCAGAGATCAGGA.........   180
5RACE-B  121 GGGTGACAGCCTCAGAGTGTTTCTTCTGCTGACAAAGACCAGAGATCAGGA.........   180

IL-28A    10 GACATGACTGGGGACTGCACGCCAGTGCTGGTGCTGATGGCCGCAGTGCTGACCGTGACT    69
IL-28B     1 ---...C.........T.....................................          57
5RACE-A  181 ..........................................................   240
5RACE-B  181 ........C.........T.....................................   240

IL-28A    70 GGAGCAGTTCCTGTCGCCAGGCTCCACGGGGCTCTCCCGGATGCAAGGGGCTGCCACATA   129
IL-28B    58 ........................G.....................................   117
5RACE-A  241 ..........................................................   300
5RACE-B  241 ........................G.....................................   300

IL-28A   130 GCCCAGTTCAAGTCCCTGTCTCCACAGGAGCTGCAGGCCTTTAAGAGGGCCAAAGATGCC   189
IL-28B   118 ..........................................................   177
5RACE-A  301 ..........................................................   357
5RACE-B  301 ..........................................................   357
```

C

```
IL-28A   421 TCAGCCCACGGCAGGGCCCAGGACCCGGGGCCGCCTCCACCATTGGCTGTACCGGCTCCA   480
IL-28B   421 ..............................................C.........   480
3RACE-A    1 ----------------------------------------------.............    15
3RACE-B    1 ----------------------------------------------...C.........    15

IL-28A   481 GGAGGCCCCAAAAAAGGAGTCCCCTGGCTGCCTCGAGGCCTCTGTCACCTTCAACCTCTT   540
IL-28B   481 ..........................................................   540
3RACE-A   16 ..........................................................    75
3RACE-B   16 ..........................................................    75

IL-28A   541 CCGCCTCCTCACGCGAGACCTGAATTGTGTTGCCAGTGGGGACCTGTGTGTCTGACCCTC   600
IL-28B   541 ..................................C.....................T   600
3RACE-A   16 ..........................................................    75
3RACE-B   16 ..................................C.....................T    75

IL-28A   601 CCACCAGTCATGCAACCTGAGATTTTATTTATAAATTAGCCACTTGTCTTAATTTATTGC   660
IL-28B   601 ..G.....................................G.....T.....T.....   660
3RACE-A   16 ..........................................................    75
3RACE-B   16 ..G.....................................G.....T.....T.....    75

IL-28A   661 CACCCAGTCGCTATTTATGTATTTGTGTGTGTAAATCCAACTCACCTCCAGGAAAATGTT   720
IL-28B   661 ........................A.....................................   720
3RACE-A   16 ..........................................................    75
3RACE-B   16 ........................A.....................................    75

IL-28A   721 TATTTTTCTACTTTTTATAACCCTTGTTGAAATAAACAA--AGGAAAAGACACTCATGAC   780
IL-28B   721 ..............GA..T.....................TG.....C.......   780
3RACE-A  256 ..........................................--...........AAAAAAA   308
3RACE-B  256 ..............GA..T.....................TG...........AAAAAAA   308
```

polyA signal — polyA tail

D

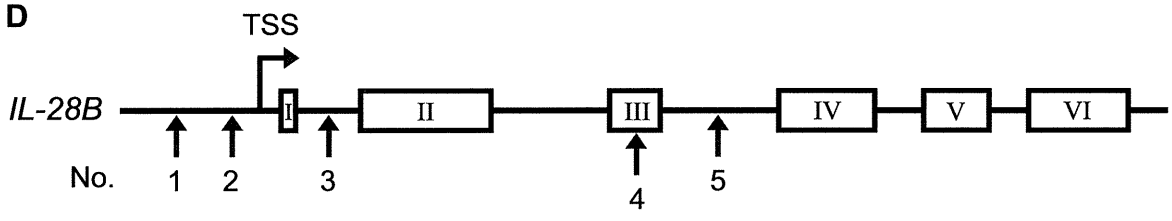

Figure 2. The determination of *IL-28B* gene structure and UTR region. *IL-28A/B* cDNA was isolated using a complete cDNA cloning method and the entire sequences were determined using HeLa, MT-2, and Raji call lines and PBMC from healthy volunteers. (A) 5′- and 3′-RACE analyses were used to determine the complete sequence of *IL-28A/B* mRNA after LPS stimulation (3 μg/mL) for 4 h following IFN-α treatment (100 U/mL) for 16 h. A representative example of agarose gel electrophoresis is shown for the non-stimulated control (NC). PCR products were inserted into the cloning vector and 6 clones of 5′- and 3′-RACE were analyzed by sequencing. (B) mRNA sequences of the 5′ terminal region were aligned using CCDS retrieved from NCBI and RACE data of *IL-28A/B*. The upper two sequences are reference sequences from the NCBI CCDS and the lower two are representative sequences of *IL-28A* and *28B* obtained from 5′-RACE. The underlined triplet indicates the start codon of each gene and arrow shows the splice junctions. (C) mRNA sequences of the 3′ terminal region were aligned using CCDS retrieved from NCBI and RACE data from *IL-28A/B*. The double-underlined triplet indicates the stop codon of each gene and arrows show the splice junctions. The polyA signal and representative site of polyadenylation also are shown. (D) The derived gene structure of the *IL-28B* is shown with the significant SNPs. The location of SNP No. 3 was changed from the regulatory to an intron region. The transcription start site (TSS) is found behind SNP No. 2.
doi:10.1371/journal.pone.0026620.g002

20 pmol of each primer, 5×PrimeSTAR GXL Buffer, 2.5 mM each deoxynucleotide triphosphates, and 1.25 units of PrimeStar GXL DNA polymerase (TAKARA Bio Inc, Tokyo, Japan). The primer pair, G1 and G2 (listed in Table S1), was used for the simultaneous amplification of the *IL-28A* and *28B* regulatory regions. The PCR conditions were as follows: 30 cycles of 10 s at 98°C, and 120 s at 68°C in addition of initial denaturation at 98°C for 5 min and a final extension at 68°C for 10 min. To separate the *IL-28A* amplicon from that of *IL-28B*, 10 μl of PCR products were analyzed using agarose gel electrophoresis and extracted with QIAquick Gel Extraction Kit (Qiagen). Each extracted product was analyzed by direct sequencing using Seq1 and Seq2 primers (Table S1). For further testing of the TA repeat, heterozygous samples were cloned into the pGEM-Teasy vector to count the number of TA repeats in each allele. Six clones were isolated and subjected to sequencing analysis using the primers described above.

Reporter assay

Luciferase assays of recombinant protein were performed using Dual-Glo Luciferase reporter assay system (Promega, Fitchburg, WI). In toll-like receptor (TLR)-stimulated experiments Raji cells were transfected and left for 16 h with 100 U/mL of IFN-α, then were exposed to LPS (3 μg/ml) for 4 h before harvesting. For assessments of recombinant protein, HeLa cells were transfected with pISRE-Luc and pGL4.74, and were harvested 24 h after IFN-α or λ treatment. The chemiluminescence was measured by SpectraMax L (Molecular Devices, Sunnyvale, CA). Firefly luciferase activity was normalized to Renilla activity to adjust for transfection efficiency.

Real-time PCR detection

Jurkat cells were transfected with the *IL-28B* expression vector harboring a FLAG sequence derived from the natural promoter (pdCMV/MA, mi, or AS). To induce IL-28B expression, TLR and IFN-α stimulation was given as described above. FLAG and glyceraldehyde-3-phosphate dehydrogenase (GAPDH) mRNA expression were measured using a real-time PCR performed on ABI Prism 7700 sequence detection system (Applied Biosystems) using primer sets (Table S1) after total RNA extraction and reverse transcription (RT) using an RT kit and TaqMan Universal PCR master mix (both Applied Biosystems), according to the manufacturer's manual. Relative gene expression was calculated as a fold induction compared to the control. Data were analyzed by the 2[-Delta Delta C(t)] method using Sequence Detector version 1.7 software (Applied Biosystems) [18] and were normalized using human GAPDH. A standard curve was prepared by serial 10-fold dilutions of human cDNA or FLAG plasmid. The curve was linear over 7 logs with a 0.998 correlation coefficient.

Statistical Analysis

Statistical analyses were conducted by using SPSS software package (SPSS 18J, SPSS, Chicago, IL) and Microsoft Excel 2007 (Microsoft co., Redmond, WA). Discrete variables were evaluated by Fisher's exact probability test. The P values were calculated by two-tailed student's t-tests for continuous data and chi-square test for categorical data, and those of less than 0.05 were considered as statistically significant.

Results

The identification of IL-28B gene structure

To define the human *IL-28A* or *IL-28B* gene structure, 5′-RACE and 3′-RACE were performed on total extracted RNA from HeLa, MT-2, Raji, HuH7 cells, and PBMCs from healthy volunteers (Fig. 2A). The sequences obtained matched the genomic contig of AC011445, which contains the sequence of *IL-28A* and *IL-28B* in forward and reverse orientations, respectively. All intron/exon junctions conformed to the canonical GT-AG rule. After stimulation of cells with LPS (3 μg/ml) for 4 h following IFN-α treatment (100 U/mL) for 16 h, *IL-28A/B* transcripts were detected in RACE experiments, but these were not detected in unstimulated cells. The representative TSSs are shown in Fig. 2B and showed little variation among cloned mRNA transcripts. The same 3′-UTR fragment also was detected without any intron in the 3′-RACE experiments (Fig. 2C). A polyadenylation signal (AAAUAAA), located in the 3′-UTR, was found upstream of the polyadenylation site in all samples. All sequences from the transcripts were aligned on the 5′-UTR, the six exons, and the 3′-UTR region of *IL-28A/B*. No different mRNA transcripts of *IL-28A/B* were found in our experiment. Taken together, the *IL-28B* gene structure comprised six exons (see Fig. 2D), and the location of SNP no. 3 (rs28416813) is in an intron, rather than a regulatory region (Table 1).

The effect of regulatory SNPs on promoter activity

Because the TSS was upstream of the position described in previous reports (Fig. 2), two rSNPs (rs72258881 and rs4803219) in the regulatory region were more specifically located in the TSS. A luciferase reporter approach was used to assess the effects of the two rSNPs on promoter activity. Luciferase vectors harboring the rSNPs were constructed and used for transfections (Fig. 3A). The promoter activities of the constructs were measured after stimulation with LPS (3 μg/ml) for 4 h following IFN-α treatment (100 U/mL) for 16 h. The transcriptional activity of constructions harboring the $(TA)_{11}$ mutation was reduced (Fig. 3B). Substitution in the rSNP (rs4803219) showed little effect on the transcriptional activity, whereas the number of TA repeats could be responsible for the putative region controlling basal transcription. To confirm the transcriptional activity, Jurkat cells were transfected with full length constructs expressing the FLAG sequence under the control of the natural promoter (Fig. 3C). To avoid the detection of endogenous mRNA, the mRNA with the FLAG sequence was specifically detected by real time PCR using the FLAG primer. The constructs harboring $(TA)_{11}$ yielded lower expression levels

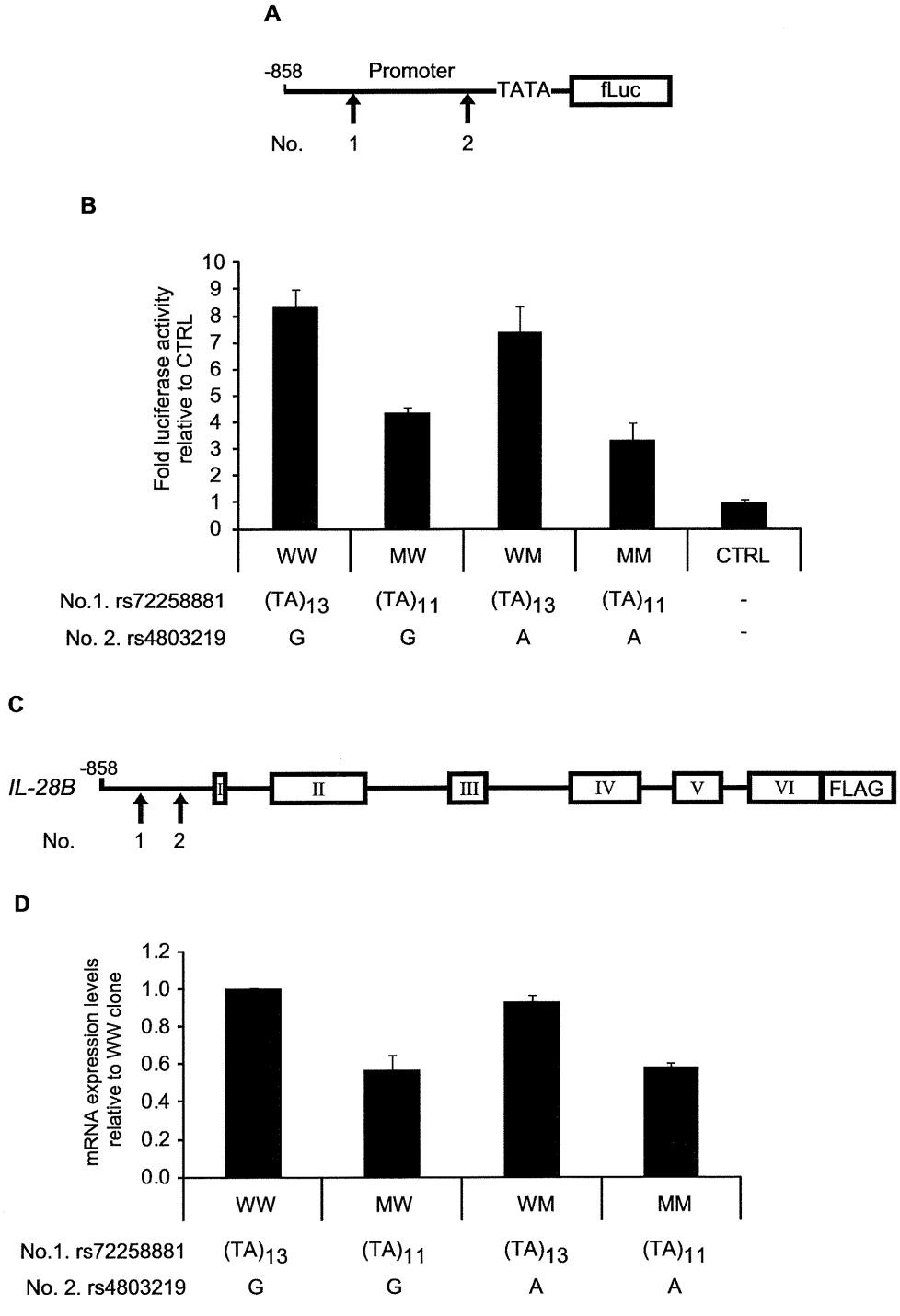

Figure 3. Transcriptional activity of the *IL-28B* promoter region compared between major and minor alleles. (A) The pGL4 reporter plasmid was constructed by subcloning the *IL-28B* promoter subfragment (nt −858 to +30). The combinations of two regulatory SNPs (rs72258881 or rs4803219) were introduced into the pGL4 vector (pGL4/WW, MW, WM, and MM). (B) Raji cells were co-transfected with pGL4 plasmids (0.05 g), and pGL4.74 control plasmid (0.05 g), and tested for firefly as well as renilla luciferase after LPS stimulation (3 μg/mL) for 4 h following IFN-α treatment (100 U/mL) for 16 h. These cells were seeded in a 96-well plate at 10^4 cells/well. The luciferase activities were normalized with renilla activities and data are presented as fold induction from activation of control vector. Bars indicate the means ± SD of triplicate determinations and the results are from one of three experiments. Statistical analyses are shown in table S2 to avoid complication. (C) For real-time PCR, the combinations of two regulatory SNPs (rs72258881 or rs4803219) were introduced into the pdCMV vector harboring a FLAG sequence (pdCMV/WW, MW, WM, and MM). (D) Jurkat cells were co-transfected with pdCMV plasmids (0.05 μg) and secreted alkaline phosphatase (SEAP) control plasmid (0.05 μg) and the expression levels were quantified using specific primer after LPS and IFN-α stimulation. The FLAG expression levels were normalized with SEAP activities and GAPDH as described in method section. Data are presented as fold induction from expression levels of pdCMV/WW. Bars indicate the means ± SD of triplicate determinations and the results are from one of three experiments. Statistical analyses are shown in table S3 to avoid complication.

doi:10.1371/journal.pone.0026620.g003

after IFN-α and LPS stimulation (Fig. 3D), suggesting that the length of TA repeat in the regulatory region of *IL-28B* could affect the regulation of *IL-28B* transcription.

Two intron SNPs located near the branch site of splicing

To determine the effect of the two iSNPs on pre-mRNA splicing, HeLa cells were transfected with wild type (WT), a construct with a double mutation of the iSNPs (d-iSNPs), or an antisense (AS) plasmid driven by the CMV promoter (Fig. 4A). The construct providing antisense transcription controlled by the CMV promoter was used to control for splicing defects (AS). Transcripts were analyzed by RT-PCR using primers in exon 1–2, 3–4, and 4–5. The RNA isolated from the WT and d-iSNPs yielded a single band using the three primer pairs. In contrast, longer amplicons were generated in cells expressing the antisense construct (Fig. 4B). The PCR products were sequenced to confirm the origin of the aberrant splicing events derived from the antisense construct (data not shown). The sequence analyses confirmed that PCR products from the WT and d-iSNPs were generated by normal splicing, suggesting that these two intron SNPs resulted in no splicing defects under these conditions.

No effect of nonsynonymous SNPs on IL-28B function

A nonsynonymous SNPs (rs8103142) located in the 3rd exon (Table 1 and Fig. 2D) led to the amino acid substitution $K^{74}R$ (Fig. 5A). Interestingly, the amino acid at this position is almost always arginine in homologous mammalian IFN-λs (e.g. human IL-28A, mouse IL-28A/B, and rhesus IL-28A/B). Then, the $K^{74}R$ substitution was expected to change IL-28B activity. The purified recombinant IL-28B protein (wild type) and the variant (ns-mut) were recognized by anti-IL-28B polyclonal antibody in a western blot assay (Fig. 5B). Based on spectrophotometric measurement of the protein concentration of the eluted fraction, it was calculated that at least 360 μg/mL of purified recombinant IL-28B protein (wild type and ns-mut) was obtained after purification. Flow-through liquid without recombinant protein was provided in the column preparing the sample of pcDNA3.1/AS (Fig. 5B). Molecular processing of IL-28B protein was confirmed to determine the precise N-terminal amino acid by peptide sequencer as the processing site of signal peptide was predicted by computer simulation (http://www.uniprot.org/uniprot/Q8IZI9). Then, the N-terminal sequence, VPVAR, was obtained (data not shown), suggesting that the simulation data was consistent with the form of physiological protein.

To evaluate the effect of nsSNPs on ISRE activity, three hepatoma cell lines (HuH7, HepG2, and HuSE2) expressing IL-28R1 and IL-10R2 were transfected with pISRE-Luc and pGL4.74. These recombinant proteins were added to the supernatant (5 ng/mL each). As shown in Fig. 5C, ISRE activity of the ns-mut protein was similar to that of wild type protein in each cell line. IFN-α (100 U/mL), as a positive control of ISRE activity, showed a strong ISRE activity. These results suggested that the nonsynonymous mutation of rs8103142 did not affect IL-28B activity *in vitro*.

The genetic variation of TA repeats at the upstream of *IL-28B*

The reference sequence (RefSeq) of the human genome in the international database registers the TA repeat SNPs, rs72284729 or rs72258881, in the regulatory regions of *IL-28A* and *IL-28B*, respectively. The registered basal number of $(TA)_n$ is 8 in the regulatory region of *IL-28A* on the plus strand, whereas that of *IL-28B* is 13 on the minus strand encoding the gene (Table 2). From 20 Japanese healthy volunteers, genomic DNA was extracted to determine the actual $(TA)_n$ number located in the region of *IL-28A* or *IL-28B* by direct sequencing and, when direct sequencing chromatographs of $(TA)_n$ heterozygotes showed mixed patterns from the end of the TA repeat (Fig. S4), the mixed samples were subjected to cloning analysis. Interestingly, the $(TA)_n$ number in *IL-28A* was consistently different from dbSNP data, whereas that of *IL-28B* showed varying numbers along with SNPs data. The $(TA)_n$ range of *IL-28B* was from 10 to 18, and the most prevalent genotype was 12/12 (75%) in healthy Japanese volunteers.

To determine the functional significance of the TA indel, the regulatory region from −858 bp to +30 bp modifying the $(TA)_n$ number was cloned into the pGL4 reporter vector, transfected into HeLa cells, and assessed for firefly luciferase reporter gene

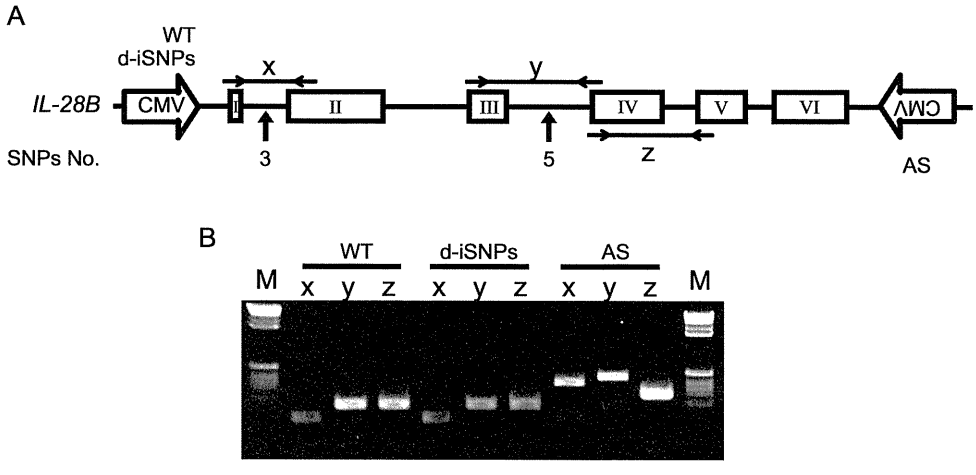

Figure 4. The determination of intron SNPs located near the branch site of splicing. (A) The expression plasmid of WT, d-iSNPs, or antisense (AS) derived from the CMV promoter was transfected into HeLa cells. Schematic of the WT, d-iSNPs, or AS used in the transfection experiments. PCR primers were designed to amplify products between exons. The effect of No. 3 and 5 SNPs (rs28416813 or rs11881222) on splicing were examined by amplicons x and y, respectively. The amplicon z was used for a splicing control. (B) Isolated RNAs were amplified by RT-PCR. The amplified products were checked by 2% agarose gel electrophoresis. The bands from the AS plasmid transcribing antisense represented abnormal splicing of mRNA as a control. Results shown are representative of three independent experiments.
doi:10.1371/journal.pone.0026620.g004

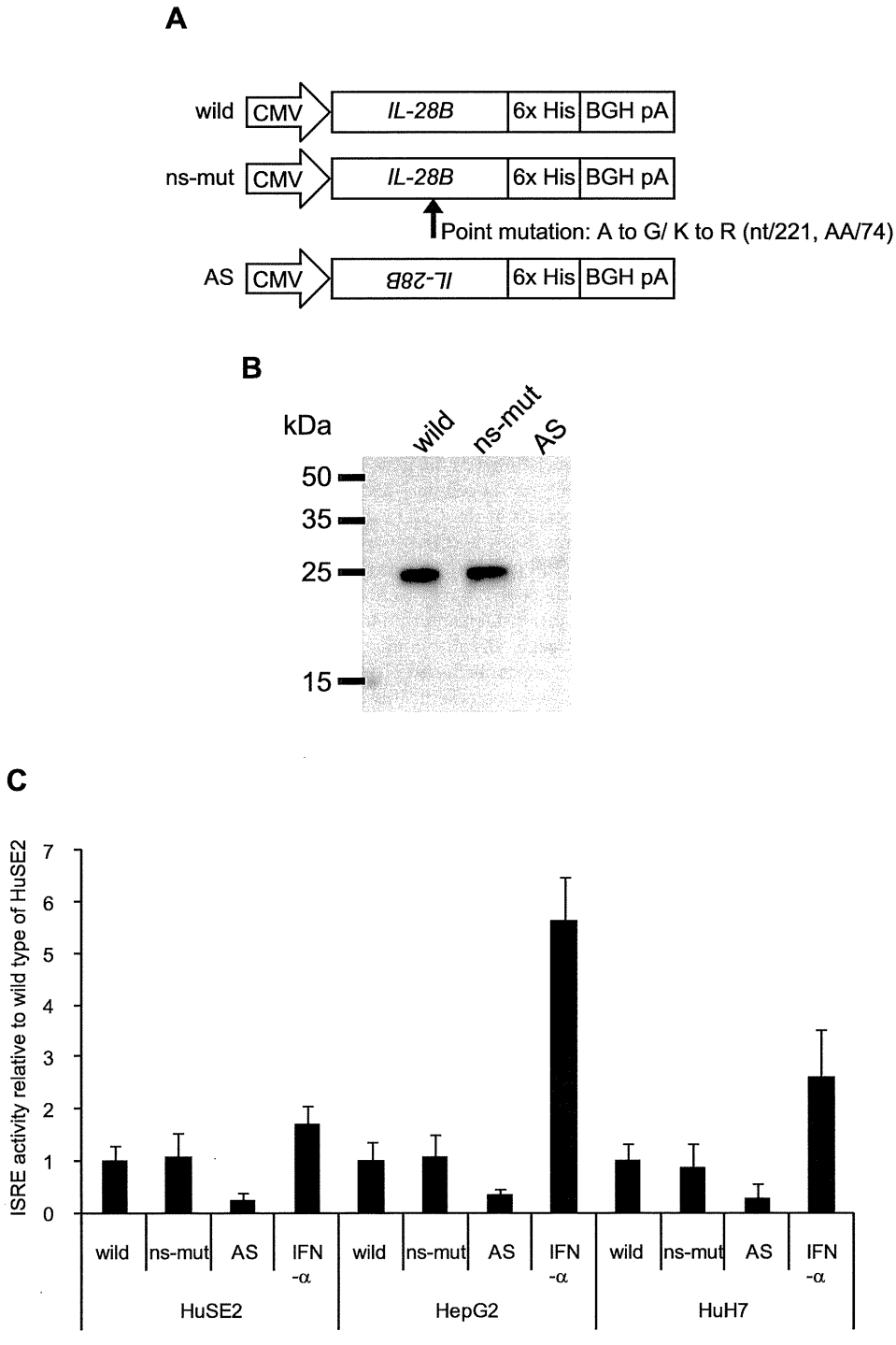

Figure 5. The purification and the activity of recombinant IL-28B with or without nsSNP. (A) The 6×His-tagged expression plasmid of wild type, ns-mut, or AS controlled by the CMV promoter was transfected into 293F cells. Schematics are the wild type, ns-mut and AS used in the transfection experiments. The procedure for recombinant protein purification is described in the materials and methods section. (B) The purified products were confirmed by immunoblotting using anti-IL28B antibody and the secondary antibody. The prepared proteins were loaded onto a 12% polyacrylamide gel. Bands corresponding to the expected molecular weight of IL-28B were observed in the wild type and ns-mut lanes. (C) For luciferase assay, HeLa cells were seeded into a 96-well plate at 10^4 cells/well and transfected with pISRE-Luc and pGL4.74 control vector before 16 h of IFN-α or IL-28B stimulation. Five ng/mL of IL-28B wild or ns-mut was added to the culture medium. Flow-though liquid from AS expression was used as a negative control. IFN-α (100 U/mL) was added for positive control of ISRE activity. The luciferase activities were normalized with Renilla activities and data are presented as fold induction from the basal promoter activation of the wild type. Bars indicate the means ± SD of triplicate determinations and the results are from one of three experiments.
doi:10.1371/journal.pone.0026620.g005

Table 2. The variations of TA repeat in *IL-28A* and *28B*.

		Location	
Gene	**Data**	**rs72284792*[1]**	**rs72258881**
IL-28A	RefSeq. (hg19)	$(TA)_8$	
	Cloning	$(TA)_8$	
IL-28B	RefSeq. (hg19)		$(TA)_{13}$
	Cloning		$(TA)_{10-18}$

*[1]The ID represents rs72258881, rs59702201, and rs67461793 because these three are located in the same genomic region, the TA repeat.
doi:10.1371/journal.pone.0026620.t002

expression (Fig. 6A). These cells were treated with 100 U/mL of IFN-α and 3 μg/mL of LPS. The results indicated that the variation in the $(TA)_n$ number at this polymorphic locus differentially regulates transcription. The transcriptional activation of the luciferase reporter gene was increased according to the $(TA)_n$ number (Fig. 6B).

Discussion

Four independent GWAS approaches have revealed the significant SNPs associated with response to PEG-IFNα/RBV therapy for CHC [12,13,14,19]. These significant SNPs were found around *IL-28B* but not *IL-28A*. The SNPs found in clinical studies to determine the outcome of HCV therapy were rs12979860 and rs8099917, because they showed the statistical significance in each study [12,13,14,19]. However, several SNPs around *IL-28B* were in strong LD (r^2>0.96) in JPT and CEU populations, although relatively low LD was predicted in the YRI population [16], and so it might be difficult to determine the most informative SNP [16]. These results suggest that any of the SNPs contained in this region could be of predictive value.

As reported in previous studies, transcription of *IL-28A/B* was upregulated in the TT genotype of rs8099917, which was associated with SVR [13,14,20], suggesting that the expression levels of *IL-28B* could be one of the key factors to clear HCV under PEG-IFNα/RBV therapy and could also affect spontaneous clearance of acute HCV infection [15]. To elucidate this question, we examined the function of the SNPs around the *IL-28B* gene to identify those SNPs affecting *IL-28B* expression. The new findings are as follows: 1) the gene structure of *IL-28B* comprised six exons in the several cell lines tested, although it was registered as having five exons in the CCDS database of NCBI. 2) The substitution of intron SNPs and non-synonymous SNPs in the *IL-28B* gene did not influence the expression levels or function. 3) Increased numbers of TA repeats in the promoter region of the *IL-28B* gene enhanced the transcription activity and expression level of the *IL-28B* gene. Because administration of IL-28B has been shown to have antiviral effects [21,22,23], lower expression of IL-28B might lead to a decrease in this effect.

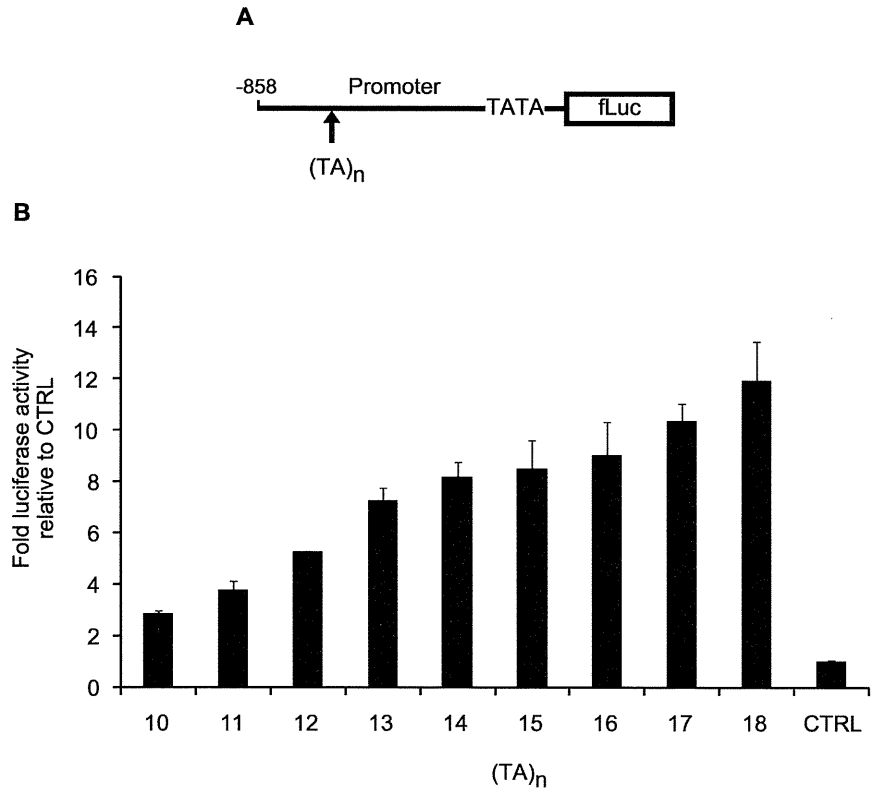

Figure 6. Luciferase assay of $(TA)_n$ number. (A) *IL-28B* promoter subfragment (nt −858 to +30) modifying $(TA)_n$ number from 10 to 18 was constructed in the pGL4 vector. (B) Raji cells were co-transfected with pGL4 plasmids (0.05 g), and pGL4.74 control plasmid (0.05 g), and tested for firefly as well as renilla luciferase after LPS stimulation (3 μg/mL) for 4 h following IFN-α treatment (100 U/mL) for 16 h. These cells were seeded into a 96-well plate at 10^4 cells/well. The luc activities were normalized with renilla activities and data are presented as fold induction from the activation of the control vector. Bars, the means ± SD of triplicate determinations and the results are from one of three experiments. Statistical analyses are shown in table S4 to avoid complication.
doi:10.1371/journal.pone.0026620.g006

The locations of two SNPs associated with response to HCV therapy, rs8099917 and rs12979860, are approximately 8 kb and 3 kb upstream of *IL-28B* gene, respectively. Because these SNPs, which showed the greatest statistical significance in the previous study, are located far from the *IL-28B* gene, another approach was required to determine the effect of the SNPs. In this study, broad $(TA)_n$ variations were observed in rs8099917 heterozygotes among CHC patients. Interestingly, a combination of TG and 11/12 genotype was strongly associated with NVR, whereas patients harboring the 12/13 genotype showed a virological response, regardless of the TG genotype (rs8099917). In clinical practice, genetic diagnosis using TA variation, following the primary classification of rs8099917 genotype, could improve the prediction of treatment response for CHC patients with the rs8099917 TG genotype. It is not clear whether the variation originates from genetic or epigenetic mechanisms. In addition, as the frequency of TA variation might be dependent on the particular population, further study will be needed to compare the frequency in several populations. A long TA repeat, over $(TA)_{13}$, was observed in healthy volunteers and showed potential for higher gene expression compared with under $(TA)_{13}$ constructs *in vitro*. It may be possible that spontaneous clearance of HCV infection and CHC patients are affected by this region because this also is dependent on *IL-28B* genotype [15,19]. In our speculation, the combination of both TA variation and the landmark SNPs, rs8099917 and rs12979860, might improve the prediction value. In addition, convenient diagnosis method to detect the TA variation like SNPs typing is needed since the present capillary techniques are relative complexity compared with SNPs typing.

In the international database, some SNPs ID are registered in the TA repeat region, located in the regulatory regions of the *IL-28A* and *IL-28B* gene, rs72284792 and rs7225881, respectively, whereas in our analysis separating *IL-28A* from *IL-28*, TA variation was detected only in the *IL-28B* region. SNP data often have been collected using next generation sequencing and based on short sequence reads. Unfortunately, the sequence similarity between *IL-28A* and *IL-28B* is over 90% from the CpG island to the region downstream of 3′-UTR. Alignment failure would occur for a high percentage of sequences when analyzed with software using general algorithms.

Effects of insertion/deletion (indel) polymorphism are known in the field of pharmacogenetic research. A polymorphism in the promoter of the uridine diphosphoglucuronosyl transferase 1A1 (*UGT 1A1*) gene has been shown to cause Crigler-Najjar syndrome types I and II and Gilbert syndrome, a benign form of unconjugated hyperbilirubinemia, and the occurrence of severe toxic events in irinotecan (known as CPT-11) administration [24,25,26]. The polymorphism consists of a $(TA)_n$ repeat in the 5′-promoter region [24,26,27], similar to that in this study. The range of repeat numbers is from $(TA)_5$ to $(TA)_8$ in the *UGT 1A1* gene [28]. The genetic disorder of the TA repeat length affects enzyme activity. The hepatic bilirubin *UGT 1A1* activity of individuals with Gilbert's syndrome is <30% of normal [29]. Irinotecan is used or under evaluation for a broad spectrum of solid tumors. Irinotecan pharmacokinetic parameters display a wide inter-patient variability and are involved in the genesis of toxic side effects [30,31,32,33]. Based on the polymorphism of the TA repeat, previous papers reported the association of irinotecan-induced severe toxicity with Gilbert's syndrome [34,35,36]. The value of genetic diagnosis of the *UGT1A1* polymorphisms prior to irinotecan chemotherapy has been corroborated in a previous study [37]. As similar characteristics were observed in the upstream region of *IL-28B*, the $(TA)_n$ repeat might be associated with disease progression as well as response to anti-HCV treatment.

In terms of epigenetic aspects, the TA variation of *IL-28B* was also suspected to be related to microsatellite instability, because a gap between the significant SNPs and TA variation was observed in this study. DNA mismatch repair (MMR) deficiency causes a high frequency of microsatellite instability (MSI-H), which is characterized by length alterations within simple repeated sequences, microsatellites. Lynch syndrome is primarily due to germline mutations in one of the DNA MMR genes, hMLH1 or hMSH2 [38]. MSI-H is also observed in <15% of colorectal, gastric and endometrial cancers, where it is associated with the hypermethylation of the promoter region of hMLH1 [39,40]. The diagnosis of MSI-H in cancers is therefore useful for identifying patients with Lynch syndrome and the efficacy of chemotherapy [41,42,43,44,45,46].

In conclusion, a (TA) dinucleotide repeat, rs72258881, located in the promoter region, was discovered by our functional studies of the proximal SNPs around *IL-28B*; the transcriptional activity of the promoter increased gradually in a $(TA)_n$ length-dependent manner. Combination diagnosis based on rs8099917 and rs72258881 might provide improved prediction because the $(TA)_n$ variation of *IL-28B* was observed but not that of *IL-28A*. The further study is needed to reveal the association with treatment response using clinical specimens of CHC. These findings suggest that the dinucleotide repeat could be associated with the transcriptional activity of *IL-28B* as well as constituting a predictor to improve prediction of the response to interferon-based HCV treatment.

Supporting Information

Figure S1 Sequence alignment of *IL-28A/B* cDNA retrieved from the database. The cDNA sequences of *IL-28A/B* were retrieved from the international database using accession number. The cDNA data reported by Sheppard et al. are AY129148 (*IL-28A*) and AY129149 (*IL-28B*) indicated with '_S' in the figure, and that of Kotenko et al. are AY184373 (*IL-28A*) and AY184374 (*IL-28B*) indicated with '_K'. Dashed boxes show the start codon predicted by computational analysis of the human genome reported by Sheppard et al. and Kotenko et al. The sequence alignment was calculated with Lasergene software (DNASTAR, Madison, WI).
(PDF)

Figure S2 Structural similarity between *IL-28A* and *IL-28B*. (A) Schematic of *IL-28A/B* gene location (UCSC genome browser). Boxes show the region representing high levels of structural similarity around *IL-28A/B*. (B) Modified schematic of structural similarity with a percentage. (C) Alignment between IL-28A and IL-28B from the CpG island to the region downstream of 3′-UTR. Homologous regions are shown by red characters. High levels of structural similarity were observed in CpG island, regulatory and gene region bypassing the in/del site.
(PDF)

Figure S3 Innate immune receptor expression related to IL-28B regulation. The relevant receptors for this study were confirmed by PCR using specific primers. (A) The mRNA expression of TLR4 was detected in cell lines, HeLa, Jurkat, MT-2, Raji, and PBMC. (B) For the study of cytokine-receptor association, the expression of IL-28RA and IL-10RB second receptor were examined using cDNA obtained from HuH7, HepG2, and HuSE2 cells. Samples without reverse transcriptase were prepared as a negative control in addition to the checking of genome contamination.
(PDF)

Figure S4 Direct sequencing analysis of TA repeat. In the first step to determine $(TA)_n$ genotypes, direct sequencing was

applied to amplicons of *IL-28A* or *28B* separated by gel electrophoresis. Homozygotes of TA repeat showed clear patterns and a high quality value in the bar above, whereas the patterns of heterozygotes were mixed because the length differed between alleles. The mixed patterns are shown in dashed boxes. These mixed products were cloned into the pGEM-Teasy vector to isolate and count the $(TA)_n$ number by sequencing of both alleles.
(PDF)

Table S1
(DOC)

Table S2
(DOC)

Table S3
(DOC)

Table S4
(DOC)

Acknowledgments

We gratefully acknowledge Dr. Naoya Sakamoto for help with reporter vector (Tokyo Medical and Dental University). We also thank the following for their technical assistance: Dr. Shuko Murakami, Ms. Hatsue Naganuma, Ms. Kyoko Akita (Nagoya City University).

Author Contributions

Conceived and designed the experiments: MS YT MN TW MM. Performed the experiments: MS YT. Analyzed the data: MS YT. Contributed reagents/materials/analysis tools: MS YT MN TW MM. Wrote the paper: MS YT MN TW MM.

References

1. Kotenko SV, Gallagher G, Baurin VV, Lewis-Antes A, Shen M, et al. (2003) IFN-lambdas mediate antiviral protection through a distinct class II cytokine receptor complex. Nat Immunol 4: 69–77.
2. Sheppard P, Kindsvogel W, Xu W, Henderson K, Schlutsmeyer S, et al. (2003) IL-28, IL-29 and their class II cytokine receptor IL-28R. Nat Immunol 4: 63–68.
3. Mordstein M, Kochs G, Dumoutier L, Renauld JC, Paludan SR, et al. (2008) Interferon-lambda contributes to innate immunity of mice against influenza A virus but not against hepatotropic viruses. PLoS Pathog 4: e1000151.
4. Sommereyns C, Paul S, Staeheli P, Michiels T (2008) IFN-lambda (IFN-lambda) is expressed in a tissue-dependent fashion and primarily acts on epithelial cells in vivo. PLoS Pathog 4: e1000017.
5. Doyle SE, Schreckhise H, Khuu-Duong K, Henderson K, Rosler R, et al. (2006) Interleukin-29 uses a type 1 interferon-like program to promote antiviral responses in human hepatocytes. Hepatology 44: 896–906.
6. Marcello T, Grakoui A, Barba-Spaeth G, Machlin ES, Kotenko SV, et al. (2006) Interferons alpha and lambda inhibit hepatitis C virus replication with distinct signal transduction and gene regulation kinetics. Gastroenterology 131: 1887–1898.
7. Zhou Z, Hamming OJ, Ank N, Paludan SR, Nielsen AL, et al. (2007) Type III interferon (IFN) induces a type I IFN-like response in a restricted subset of cells through signaling pathways involving both the Jak-STAT pathway and the mitogen-activated protein kinases. J Virol 81: 7749–7758.
8. Bartlett NW, Buttigieg K, Kotenko SV, Smith GL (2005) Murine interferon lambdas (type III interferons) exhibit potent antiviral activity in vivo in a poxvirus infection model. J Gen Virol 86: 1589–1596.
9. Brand S, Zitzmann K, Dambacher J, Beigel F, Olszak T, et al. (2005) SOCS-1 inhibits expression of the antiviral proteins 2′,5′-OAS and MxA induced by the novel interferon-lambdas IL-28A and IL-29. Biochem Biophys Res Commun 331: 543–548.
10. Robek MD, Boyd BS, Chisari FV (2005) Lambda interferon inhibits hepatitis B and C virus replication. J Virol 79: 3851–3854.
11. Zhu H, Butera M, Nelson DR, Liu C (2005) Novel type I interferon IL-28A suppresses hepatitis C viral RNA replication. Virol J 2: 80.
12. Ge D, Fellay J, Thompson AJ, Simon JS, Shianna KV, et al. (2009) Genetic variation in IL28B predicts hepatitis C treatment-induced viral clearance. Nature 461: 399–401.
13. Suppiah V, Moldovan M, Ahlenstiel G, Berg T, Weltman M, et al. (2009) IL28B is associated with response to chronic hepatitis C interferon-alpha and ribavirin therapy. Nat Genet 41: 1100–1104.
14. Tanaka Y, Nishida N, Sugiyama M, Kurosaki M, Matsuura K, et al. (2009) Genome-wide association of IL28B with response to pegylated interferon-alpha and ribavirin therapy for chronic hepatitis C. Nat Genet 41: 1105–1109.
15. Thomas DL, Thio CL, Martin MP, Qi Y, Ge D, et al. (2009) Genetic variation in IL28B and spontaneous clearance of hepatitis C virus. Nature 461: 798–801.
16. Tanaka Y, Nishida N, Sugiyama M, Tokunaga K, Mizokami M (2010) lambda-Interferons and the single nucleotide polymorphisms: A milestone to tailor-made therapy for chronic hepatitis C. Hepatol Res 40: 449–460.
17. Siren J, Pirhonen J, Julkunen I, Matikainen S (2005) IFN-alpha regulates TLR-dependent gene expression of IFN-alpha, IFN-beta, IL-28, and IL-29. J Immunol 174: 1932–1937.
18. Livak KJ, Schmittgen TD (2001) Analysis of relative gene expression data using real-time quantitative PCR and the 2(-Delta Delta C(T)) Method. Methods 25: 402–408.
19. Rauch A, Kutalik Z, Descombes P, Cai T, Di Iulio J, et al. (2010) Genetic variation in IL28B is associated with chronic hepatitis C and treatment failure: a genome-wide association study. Gastroenterology. pp 138–1338–1345, 1345 e1331–1337.
20. Fukuhara T, Taketomi A, Motomura T, Okano S, Ninomiya A, et al. (2010) Variants in IL28B in liver recipients and donors correlate with response to peg-interferon and ribavirin therapy for recurrent hepatitis C. Gastroenterology. pp 139–1577–1585, 1585 e1571–1573.
21. Ank N, Iversen MB, Bartholdy C, Staeheli P, Hartmann R, et al. (2008) An important role for type III interferon (IFN-lambda/IL-28) in TLR-induced antiviral activity. J Immunol 180: 2474–2485.
22. Ank N, West H, Bartholdy C, Eriksson K, Thomsen AR, et al. (2006) Lambda interferon (IFN-lambda), a type III IFN, is induced by viruses and IFNs and displays potent antiviral activity against select virus infections in vivo. J Virol 80: 4501–4509.
23. Contoli M, Message SD, Laza-Stanca V, Edwards MR, Wark PA, et al. (2006) Role of deficient type III interferon-lambda production in asthma exacerbations. Nat Med 12: 1023–1026.
24. Bosma PJ, Chowdhury JR, Bakker C, Gantla S, de Boer A, et al. (1995) The genetic basis of the reduced expression of bilirubin UDP-glucuronosyltransferase 1 in Gilbert's syndrome. N Engl J Med 333: 1171–1175.
25. Monaghan G, Ryan M, Seddon R, Hume R, Burchell B (1996) Genetic variation in bilirubin UPD-glucuronosyltransferase gene promoter and Gilbert's syndrome. Lancet 347: 578–581.
26. Raijmakers MT, Jansen PL, Steegers EA, Peters WH (2000) Association of human liver bilirubin UDP-glucuronyltransferase activity with a polymorphism in the promoter region of the UGT1A1 gene. J Hepatol 33: 348–351.
27. Sato H, Adachi Y, Koiwai O (1996) The genetic basis of Gilbert's syndrome. Lancet 347: 557–558.
28. Beutler E, Gelbart T, Demina A (1998) Racial variability in the UDP-glucuronosyltransferase 1 (UGT1A1) promoter: a balanced polymorphism for regulation of bilirubin metabolism? Proc Natl Acad Sci U S A 95: 8170–8174.
29. Yamamoto K, Sato H, Fujiyama Y, Doida Y, Bamba T (1998) Contribution of two missense mutations (G71R and Y486D) of the bilirubin UDP glycosyltransferase (UGT1A1) gene to phenotypes of Gilbert's syndrome and Crigler-Najjar syndrome type II. Biochim Biophys Acta 1406: 267–273.
30. Gupta E, Lestingi TM, Mick R, Ramirez J, Vokes EE, et al. (1994) Metabolic fate of irinotecan in humans: correlation of glucuronidation with diarrhea. Cancer Res 54: 3723–3725.
31. Gupta E, Mick R, Ramirez J, Wang X, Lestingi TM, et al. (1997) Pharmacokinetic and pharmacodynamic evaluation of the topoisomerase inhibitor irinotecan in cancer patients. J Clin Oncol 15: 1502–1510.
32. Rowinsky EK, Grochow LB, Ettinger DS, Sartorius SE, Lubejko BG, et al. (1994) Phase I and pharmacological study of the novel topoisomerase I inhibitor 7-ethyl-10-[4-(1-piperidino)-1-piperidino]carbonyloxycamptothecin (CPT-11) administered as a ninety-minute infusion every 3 weeks. Cancer Res 54: 427–436.
33. Iyer L, King CD, Whitington PF, Green MD, Roy SK, et al. (1998) Genetic predisposition to the metabolism of irinotecan (CPT-11). Role of uridine diphosphate glucuronosyltransferase isoform 1A1 in the glucuronidation of its active metabolite (SN-38) in human liver microsomes. J Clin Invest 101: 847–854.
34. Sugatani J, Yamakawa K, Yoshinari K, Machida T, Takagi H, et al. (2002) Identification of a defect in the UGT1A1 gene promoter and its association with hyperbilirubinemia. Biochem Biophys Res Commun 292: 492–497.
35. Iyanagi T, Emi Y, Ikushiro S (1998) Biochemical and molecular aspects of genetic disorders of bilirubin metabolism. Biochim Biophys Acta 1407: 173–184.
36. Wasserman E, Myara A, Lokiec F, Goldwasser F, Trivin F, et al. (1997) Severe CPT-11 toxicity in patients with Gilbert's syndrome: two case reports. Ann Oncol 8: 1049–1051.
37. Sadee W, Dai Z (2005) Pharmacogenetics/genomics and personalized medicine. Hum Mol Genet 14 Spec No. 2: R207-214.
38. Modrich P (1994) Mismatch repair, genetic stability, and cancer. Science 266: 1959–1960.
39. Lengauer C, Kinzler KW, Vogelstein B (1997) DNA methylation and genetic instability in colorectal cancer cells. Proc Natl Acad Sci U S A 94: 2545–2550.

40. Lengauer C, Kinzler KW, Vogelstein B (1997) Genetic instability in colorectal cancers. Nature 386: 623–627.
41. Kim GP, Colangelo LH, Paik S, O'Connell MJ, Kirsch IR, et al. (2007) Predictive value of microsatellite instability-high remains controversial. J Clin Oncol 25: 4857; author reply 4857–4858.
42. Elsaleh H, Joseph D, Grieu F, Zeps N, Spry N, et al. (2000) Association of tumour site and sex with survival benefit from adjuvant chemotherapy in colorectal cancer. Lancet 355: 1745–1750.
43. Gryfe R, Kim H, Hsieh ET, Aronson MD, Holowaty EJ, et al. (2000) Tumor microsatellite instability and clinical outcome in young patients with colorectal cancer. N Engl J Med 342: 69–77.
44. Ribic CM, Sargent DJ, Moore MJ, Thibodeau SN, French AJ, et al. (2003) Tumor microsatellite-instability status as a predictor of benefit from fluorouracil-based adjuvant chemotherapy for colon cancer. N Engl J Med 349: 247–257.
45. Popat S, Hubner R, Houlston RS (2005) Systematic review of microsatellite instability and colorectal cancer prognosis. J Clin Oncol 23: 609–618.
46. Sinicrope FA, Rego RL, Halling KC, Foster N, Sargent DJ, et al. (2006) Prognostic impact of microsatellite instability and DNA ploidy in human colon carcinoma patients. Gastroenterology 131: 729–737.

Hepatitis C Virus Reveals a Novel Early Control in Acute Immune Response

Noëlla Arnaud[1], Stéphanie Dabo[1], Daisuke Akazawa[2], Masayoshi Fukasawa[3], Fumiko Shinkai-Ouchi[3], Jacques Hugon[4], Takaji Wakita[2], Eliane F. Meurs[1]*

1 Institut Pasteur, Hepacivirus and Innate Immunity, Paris, France, **2** National Institute of Infectious Diseases, Department of Virology II, Tokyo, Japan, **3** National Institute of Infectious Diseases, Department of Biochemistry and Cell Biology, Tokyo, Japan, **4** Institut du Fer à Moulin, INSERM UMRS 839, Paris, France

Abstract

Recognition of viral RNA structures by the intracytosolic RNA helicase RIG-I triggers induction of innate immunity. Efficient induction requires RIG-I ubiquitination by the E3 ligase TRIM25, its interaction with the mitochondria-bound MAVS protein, recruitment of TRAF3, IRF3- and NF-κB-kinases and transcription of Interferon (IFN). In addition, IRF3 alone induces some of the Interferon-Stimulated Genes (ISGs), referred to as early ISGs. Infection of hepatocytes with Hepatitis C virus (HCV) results in poor production of IFN despite recognition of the viral RNA by RIG-I but can lead to induction of early ISGs. HCV was shown to inhibit IFN production by cleaving MAVS through its NS3/4A protease and by controlling cellular translation through activation of PKR, an eIF2α-kinase containing dsRNA-binding domains (DRBD). Here, we have identified a third mode of control of IFN induction by HCV. Using HCVcc and the Huh7.25.CD81 cells, we found that HCV controls RIG-I ubiquitination through the di-ubiquitine-like protein ISG15, one of the early ISGs. A transcriptome analysis performed on Huh7.25.CD81 cells silenced or not for PKR and infected with JFH1 revealed that HCV infection leads to induction of 49 PKR-dependent genes, including ISG15 and several early ISGs. Silencing experiments revealed that this novel PKR-dependent pathway involves MAVS, TRAF3 and IRF3 but not RIG-I, and that it does not induce IFN. Use of PKR inhibitors showed that this pathway requires the DRBD but not the kinase activity of PKR. We then demonstrated that PKR interacts with HCV RNA and MAVS prior to RIG-I. In conclusion, HCV recruits PKR early in infection as a sensor to trigger induction of several IRF3-dependent genes. Among those, ISG15 acts to negatively control the RIG-I/MAVS pathway, at the level of RIG-I ubiquitination.These data give novel insights in the machinery involved in the early events of innate immune response.

Citation: Arnaud N, Dabo S, Akazawa D, Fukasawa M, Shinkai-Ouchi F, et al. (2011) Hepatitis C Virus Reveals a Novel Early Control in Acute Immune Response. PLoS Pathog 7(10): e1002289. doi:10.1371/journal.ppat.1002289

Editor: Aleem Siddiqui, University of California, San Diego, United States of America

Received April 5, 2011; **Accepted** August 13, 2011; **Published** October 13, 2011

Copyright: © 2011 Arnaud et al. This is an open-access article distributed under the terms of the Creative Commons Attribution License, which permits unrestricted use, distribution, and reproduction in any medium, provided the original author and source are credited.

Funding: NA was supported by a graduate fellowship from the Ministry of Research and Technology. The work was supported by grants from the Pasteur Institute and by grant R750159 from ANRS (Agence Nationale de la Recherche sur le SIDA et les Hepatites Virales):http://www.anrs.fr The funders had no role in study design, data collection and analysis, decision to publish, or preparation of the manuscript.

Competing Interests: The authors have declared that no competing interests exist.

* E-mail: emeurs@pasteur.fr

Introduction

IFN induction in response to several RNA viruses involves the intracytosolic pathogen recognition receptor (PRR) CARD-containing DexD/H RNA helicase RIG-I. Following its binding to viral RNA, RIG-I undergoes a change in its conformation through Lys63-type ubiquitination by the E3 ligase TRIM25. This allows its N-terminal CARD domain to interact with the CARD domain of the mitochondria-bound adapter MAVS [1,2]. MAVS then interacts with TRAF3 to further recruit downstream IRF3 and NF-κB-activating kinases, that stimulate the IFNβ promoter in a cooperative manner. In addition, IRF3 stimulates directly the promoters of some interferon-induced genes (early ISGs) while NF-κB stimulates that of inflammatory cytokines [3].

The RNA of Hepatitis C virus (HCV) has an intrinsic ability to trigger IFNβ induction through RIG-I [4,5,6]. Yet HCV is a poor IFN inducer. One reason for this comes from the ability of its NS3 protease to cleave MAVS [7]. Another relates to the ability of HCV to trigger activation of the dsRNA-dependent eIF2α kinase PKR [8,9] which leads to inhibition of IFN expression through general control of translation while the viral genome can be translated from its eIF2α-insensitive IRES structure [8].

HCV infection can trigger important intrahepatic synthesis of several IFN-induced genes (ISGs) in patients [10,11] and in animal models of infection in chimpanzees [12]. Expression of ISGs can be explained at least in part by the ability of HCV to activate the IFN-producing pDCs in the liver through cell-to-cell contact with HCV-infected cells [13]. Intriguingly, despite the recognized antiviral activity of a number of these ISGs, their high expression paradoxically represents a negative predictive marker for the response of these patients to standard combination IFN/ribavirin therapy [14,15,16]. The ubiquitine-like protein ISG15 is among the ISGs which are the most highly induced by HCV [16] and was recently shown to act as a pro-HCV agent [17]. Interestingly, ISG15 was also shown to control RIG-I activity through ISGylation [18].

Here, we show that HCV controls IFN induction at the level of RIG-I ubiquitination through the ubiquitine-like protein ISG15, one of the early ISGs. Use of small interfering RNA (siRNA) targeting to compare the effect of ISG15 to that of PKR on IFN induction and HCV replication led to the unexpected finding that HCV infection triggers induction of ISG15 and other ISGs by using PKR as an adapter through its N terminal dsRNA binding domain. This recruits a signaling pathway which involves MAVS,TRAF3

Author Summary

Hepatitis C Virus (HCV) is a poor interferon (IFN) inducer, despite recognition of its RNA by the cytosolic RNA helicase RIG-I. This is due in part through cleavage of MAVS, a downstream adapter of RIG-I, by the HCV NS3/4A protease and through activation of the eIF2α-kinase PKR to control IFN translation. Here, we show that HCV also inhibits RIG-I activation through the ubiquitin-like protein ISG15 and that HCV triggers rapid induction of 49 genes, including ISG15, through a novel signaling pathway that precedes RIG-I and involves PKR as an adapter to recruit MAVS. Hence, we propose to divide the acute response to HCV infection into one early (PKR) and one late (RIG-I) phase, with the former controlling the latter. Furthermore, these data emphazise the need to check compounds designed as immune adjuvants for activation of the early acute phase before using them to sustain innate immunity.

and IRF3 but not RIG-I. Altogether, our results present a novel mechanism by which HCV uses PKR and ISG15 to attenuate the innate immune response.

Results

HCV infection negatively controls RIG-I ubiquitination

We recently reported that the HCV permissive Huh7.25.CD81 cells [19] that we used to identify the pro-HCV action of PKR, did not induce IFN in response to HCV infection, unless after ectopic expression of TRIM25 [8]. We started this study by investigating at which level this defect could occur. A $P_{358}L$ substitution in the endogenous TRIM25 of these cells, revealed by sequence analysis, proved to have no incidence of the ability of TRIM25 to participate in the IFN induction process. Indeed, ectopic expression of a TRIM25 $P_{358}L$ construct was as efficient as a TRIM25wt construct to increase IFN induction in the Huh7.25.CD81 cells, after infection with Sendai virus (SeV) (**Figure 1A**). Like some other members of the TRIM family, TRIM25 is localized in both the cytosol and nucleus and is induced upon IFN treatment [20]. No specific difference between the cellular localization of TRIM25 was observed in the Huh7.25.CD81 cells when compared to Huh7 cells or Huh7.5 cells, which rules out a role for a cellular mislocalization in its inability to participate in IFN induction (**Figure 1B**). TRIM25 was also efficiently induced by IFN (**Figure 1B and Figure S1**). We assayed whether increasing TRIM25 upon IFN treatment could mimic the effect of its ectopic expression and restore IFN induction in response to HCV infection. However, this resulted only in a poor stimulation of an IFNβ promoter (3 to 5-fold), in contrast to its effect upon SeV infection (230-fold) (**Figure 1C**). Similarly, HCV infection at higher m.o.i, as an attempt to favour recognition of RIG-I by the viral RNA, only modestly increased IFN induction (**Figure 1D**). TRIM25 plays an essential role in IFN induction through RIG-I ubiquitination [1]. We then analysed whether this step was affected by HCV infection in the Huh7.25.CD81 cells. The results showed that, in contrast to SeV infection used as control, HCV infection could not trigger RIG-I ubiquitination, unless the cells are supplied with ectopic TRIM25 (**Figure 1E**). Thus, HCV infection appears to mediate a control on IFN induction through regulation of RIG-I ubiquitination.

HCV controls RIG-I ubiquitination through ISG15

Inhibition of the function of TRIM25 or RIG-I ubiquitination has been suggested to occur via the small ubiquitin-like protein ISG15 and the process of ISGylation [18,21]. We then analysed whether ISG15 was involved in the control of RIG-I ubiquitination upon HCV infection. For this, we chose a transient transfection approach using siRNAs targeting ISG15 in the Huh7.25.CD81 cells. Indeed, this resulted in a strong ubiquitination of RIG-I at 9 hrs and 12 hrs post-HCV infection, which was equivalent to that observed in cells supplied with ectopic TRIM25 (**Figure 2A**). A similar result was obtained after JFH1 infection in the Huh7 cells, used as another HCV-permissive cell line (**Figure S2**). Thus, ISG15 can control RIG-I ubiquitination in different cells infected by HCV. We next investigated whether ISGylation was involved in this process. Absence of detection of RIG-I ubiquitination after HCV infection of the Huh7.25.CD81 cells precludes direct analysis of the effect of ISG15 on RIG-I. We used an IFNβ-luc reporter assay instead, as it proved to be sensitive enough to detect some IFN induction in response to JFH1 infection in those cells (see Figure 1D). We found that IFN induction increased when cells were transfected with siRNAs targeting ISG15 while it decreased in cells overexpressing IGS15 (**Figure 2B**). Expression of ISG15 in the presence of the E1, E2 and E3 ligases involved in ISGylation (respectively Ube1L, UbcH8 and HERC5) [22] further inhibits IFNβ induction (**Figure 2B**). Similar results were observed upon infection with Sendai virus (**Figure S3**). The ISGylation process is strictly dependent on the presence of the E1 ligase Ube1L [23]. Indeed, enhanced IFN promoter activity has been observed in Ube1L−/− cells in response to NDV [18]. In accord with this, depletion of endogenous Ube1L from the Huh7.25.CD81 cells (**Figure S4**), as such or after ectopic expression of ISG15, UbcH8 and HERC5, resulted in an increase in IFNβ induction after infection with HCV (**Figure 2B**). We then analysed the effect of siISG15 on IFNβ induction after infecting the cells with HCV up to 72 hours, in order to pass through the 24 hr time-point where the signaling pathway leading to the transcription of this gene is expected to stop because of the NS3/4A-mediated cleavage of MAVS [8]. The results show that, whereas IFNβ transcription was indeed strongly inhibited after 24 hr in the control cells, it still occurred significantly in the cells expressing siRNA ISG15 (**Figure 2C**). Previous data have shown a positive role for ISG15 on HCV production [24,25]. In accord with this, silencing of ISG15 resulted in clear inhibition of HCV RNA expression with however no significant consequence on the ability of the virions produced to re-infect fresh cells (**Figure 2D**). Analysis of expression of MAVS and NS3, as well as the expression of the core protein as another example of viral protein, then showed that the depletion of ISG15 both decreased and delayed the expression of the viral proteins as compared to the siRNA control cells and that this was correlated by a delay in the NS3/4A-mediated cleavage of MAVS (**Figure 2E**). These results show that ISG15 controls the process of IFN induction during HCV infection by interfering with RIG-I ubiquitination through an ISGylation process and by boosting efficient accumulation of NS3, among other viral proteins, thus favouring its negative control on IFN induction by cleavage of MAVS.

ISG15 strengthens the pro-HCV activity of PKR

ISG15 ([24,25] and this study) and PKR [8,9] emerge as two ISGs with pro-HCV activities, instead of playing an antiviral role. We then assayed the effect of a combined depletion of PKR and ISG15 on HCV replication and IFN expression in the Huh7.25.CD81 cells. As shown in Figure 2 D and B, siRNAs targeting ISG15 were sufficient both to inhibit HCV replication (**Figure 3A**) and to increase IFNβ expression, either measured by RTqPCR (**Figure 3B**) or by using an IFNβ-luciferase reporter

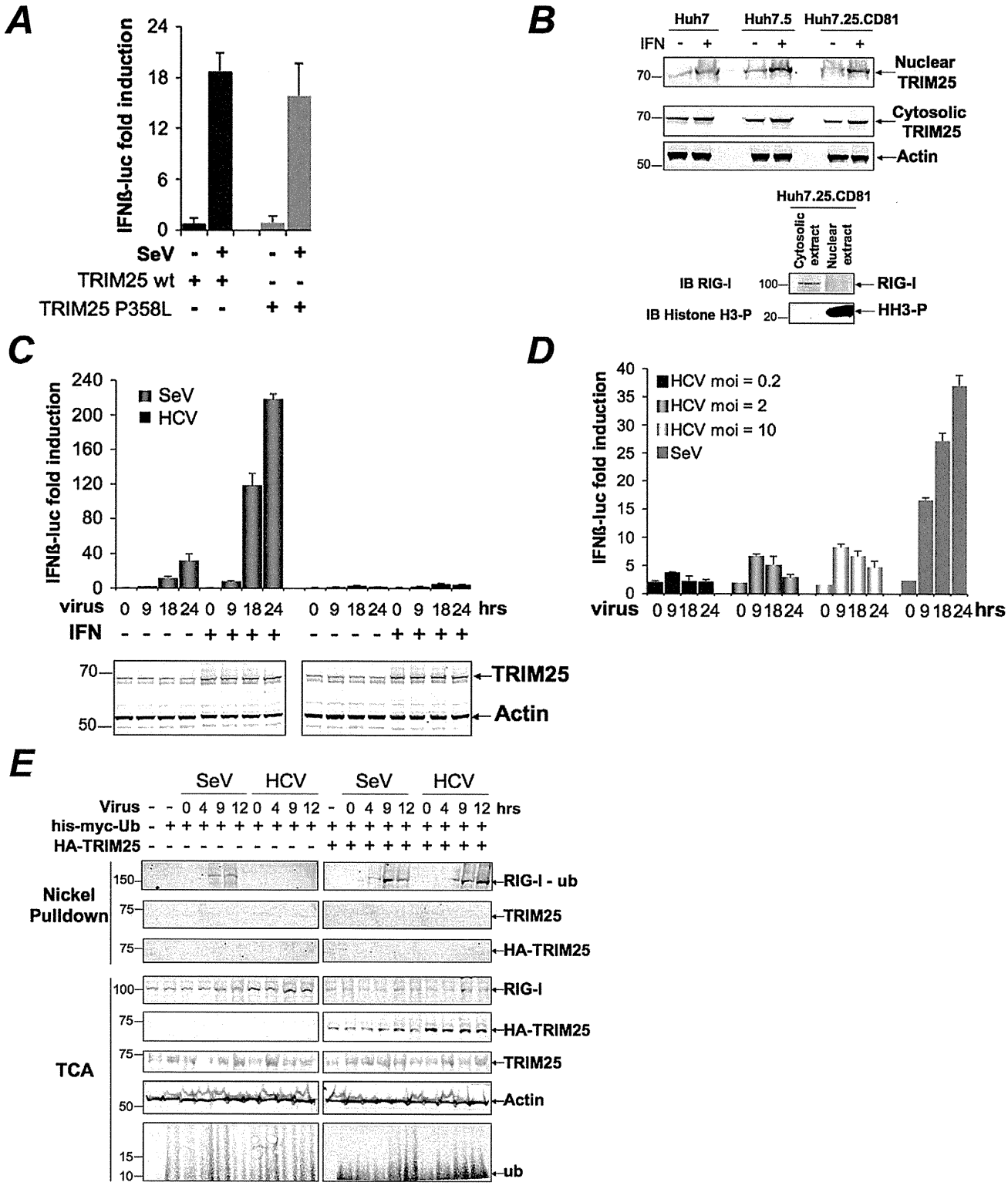

Figure 1. HCV infection negatively controls RIG-I ubiquitination. (**A**) Huh7.25.CD81 cells were transfected for 24 hrs with 150 ng of the pGL2-IFNβ-FLUC; 40 ng of the pRL-TK-RLUC reporter plasmids alone or in presence of 150 ng of a plasmid expressing HA-TRIM25, either as such (TRIM25wt) or containing the $P_{358}L$ substitution (a SNP rs75467764 with no reported pathology). Cells were infected or not with SeV (40 HAU/ml) for 24 hrs. IFN expression was expressed as fold induction of luciferase activity. Error bars represent the mean ± S.D. for triplicates. (**B**) Huh7, Huh7.5 and Huh7.25.CD81 cells were either untreated or treated with 500 U/ml IFNα for 24 hrs. TRIM25 was detected by immunoblot after preparation of nuclear and cytosolic fractions from 25 µg of cell extracts. Detection of Actin, RIG-I and phosphorylated Histone 3 (HH3-P) served as controls. (**C–D**) Huh7.25.CD81 cells were transfected with the reporter plasmids as in A, a few hours before being treated with 500 U/ml IFNα for 24 hrs (**C**) or left untreated (**C or D**). They were then infected with Sendai virus (40 HAU/ml) or with JFH1 at an m.o.i of 0.2 (**C**) or increasing from 0.2 to 10 (**D**). At the times indicated, IFN expression was expressed as fold induction of luciferase activity. Error bars represent the mean ± S.D. for triplicates. Induction of

TRIM25 after IFN treatment was shown by immunoblot (**C**). (**E**) The Huh7.25.CD81 cells were transfected for 48 hrs with 5 μg of His-Myc-Ubiquitin expression plasmid in absence or presence of a plasmid expressing HA-TRIM25 and infected with SeV (40 HAU/ml) or HCV (m.o.i = 6). At the times indicated, 10% of the lysate was precipitated with TCA and the remaining lysate subjected to nickel pulldown under denaturing conditions. Total and ubiquitin (Ub)-modified proteins were separated by SDS-PAGE and revealed by immunoblot.
doi:10.1371/journal.ppat.1002289.g001

assay (**Figure 3C**). Very limited additional effect was observed in the concomitant presence of siRNAs targeting PKR. (**Figure 3B**). Interestingly, we noticed that expression of luciferase from the IFNβ promoter increased throughout the first 18 hours of HCV infection in the siISG15 cells (**Figure 3C**). This was intriguing as it should have been inhibited after 12 hours of HCV infection through the eIF2α kinase activity of PKR and its control on translation [8]. We therefore analysed whether the state of PKR activation (phosphorylation) was dependent on the expression of ISG15. For this, the Huh7.25.CD81 cells were transfected either with siRNAs targeting ISG15 or with a plasmid expressing an HA-ISG15 construct and PKR phosphorylation was analysed as described previously [8]. The results showed that depletion of ISG15 inhibits PKR activation in the HCV-infected cells, while its overexpression stimulates it (**Figure 3D** and **Figure S5**). Therefore these data reveal that, in addition to negatively controlling RIG-I ubiquitination, ISG15 can also positively control PKR activity. The conjugation of both effects results in an efficient control of IFN induction during HCV infection.

HCV triggers a PKR-dependent pathway early in infection to induce ISG15 and other genes

The Huh7.25.CD81 cells express ISG15 at significant basal levels. This situation was not surprising as various cellular systems can also express some of the ISGs at basal level. Expression of ISG15 was approximately 2- and 5-fold higher in the Huh7.25.CD81 cells than in the Huh7.5 or Huh7 cells (data not shown). Intriguingly however, we noticed that ISG15 expression was increased in response to HCV infection (see **Figure 2E**). To investigate this further, we simply re-used the RNAs prepared for the experiment shown in Figure 3B and performed a quantitative kinetics analysis. The results confirmed that HCV can trigger induction of ISG15 (**Figure 4A**). Unexpectedly, analysis of the RNA extracted from the cells treated with siRNAs targeting PKR, revealed that ISG15 RNA expression was strongly repressed when PKR was silenced (**Figure 4A**). This surprising result was confirmed by analysing induction of ISG56, another early ISG [26], both at the level of its endogenous RNA (**Figure 4B**) or by using an ISG56-luciferase vector (**Figure 4C**). In the latter case, a strong increase of the reporter expression in the cells treated with siRNAs targeting ISG15, was similar to the situation observed for IFNβ RNA (**Figure 2B and 2C**). This can be related to activation of the RIG-I pathway, which can function when ISG15 is absent. These data suggest that HCV may use PKR to activate gene transcription. Importantly, this phenomenon was specific to HCV as infection with Sendai virus resulted in a similar induction of ISG15 and ISG56, regardless of PKR (**Figure 4D and Figure S6**). We then examined whether overexpression of PKR could boost induction of ISG15 during HCV infection and how this would affect HCV replication and IFN induction, in relation to the pro-HCV action of ISG15. Huh7.25.CD81 cells were transfected with a plasmid expressing PKR alone or in presence of siRNAs targeting ISG15, before being infected with HCV over 48 hours. Overexpression of PKR increased the ability of HCV to induce ISG15 and concomitantly, led to an increase in HCV RNA expression. The latter increase was abolished when ISG15 was silenced, thus showing that the PKR-dependent increase in HCV expression is mediated by ISG15 (Figure **4E**). However, while the cells silenced for ISG15 are able to induce IFN in response to HCV infection, as shown in Figure 3B, they are unable to do so when PKR is overexpressed. This suggests that PKR may also interfere with the process of IFN induction, independently of ISG15, a possibility that remains to be explored.

A role for PKR in gene induction in response to HCV infection has not been described before. Additional information was therefore obtained through a transcriptome analysis of 2165 genes in the Huh7.25.CD81 cells treated with control siRNAs or siRNAs targeting PKR and infected with HCV for 12 hrs. Out of the most significant 422 genes that were identified, 99 were unmodified or barely modified and 33 were down-regulated, while 290 genes were found to be up-regulated by HCV infection (data not shown). Among those, HCV infection triggered up-regulation of 49 genes which are directly dependent on PKR expression (**Table 1**). Forty percent of these genes (20) belong to the family of the ISGs, with ISG15 among the most induced genes (**Table 1**). In the reciprocal situation, only 17 genes depended on PKR for their down-regulation by HCV infection, with no link to a particular family of genes and limited variation both in number and intensity (**Table S1**). Thus, induction of ISGs upon HCV infection may occur through a novel signaling pathway that involves PKR.

Induction of ISG15 by HCV is independent of RIG-I, involves MAVS/TRAF3 association with PKR and involves the DRBD region but not the catalytic activity of PKR

Infection with RNA viruses or transient transfection with dsRNA can directly and rapidly induce early ISGs, such as ISG15, through IRF3, after activation of the RIG-I/MAVS pathway and recruitment of TRAF3, an essential adapter which recruits the downstream IRF3 kinases TBK1/IKKε. We have shown that the RIG-I pathway was not operative during HCV infection in the Huh7.25.CD81 cells, precisely due to the presence of ISG15. To determine how ISG15 induction through PKR relates to or differs from the RIG-I/MAVS pathway, the Huh7.25.CD81 cells were treated with siRNAs aimed at targeting separately PKR, RIG-I, MAVS, TRAF3 and IRF3 (**Figure S7**) and infected with HCV. The results clearly showed that induction of ISG15 in response to HCV infection depends on PKR, MAVS, TRAF3 and IRF3 but not on RIG-I (**Figure 5A**). The participation of IRF3 was further confirmed by immunofluorescence studies which showed its nuclear translocation at 6 hours post-infection (**Figure S8**). ISG15, as well as ISG56, was also clearly induced in response to HCV infection in two other HCV permissive cell lines, such as Huh7 and Huh7.5 cells, and this induction was abrogated in presence of siRNAs targeting PKR (**Figure 5B and Figure S9**). Importantly, since Huh7.5 cells express a non-functional RIG-I/MAVS pathway due to a mutation in RIG-I, result with these cells supports the notion that the ability of HCV to trigger induction of ISGs through PKR is independent of RIG-I. To have more insights on this novel PKR signaling pathway, PKR was immunoprecipitated at early times points following infection of Huh7.25.CD81 cells with HCV and the immunocomplexes were analysed for the presence of MAVS, TRAF3 and RIG-I. Both MAVS and TRAF3, but not RIG-I, associate with PKR in a time dependent manner, beginning at 2 hrs post-infection (**Figure 5C**). Strikingly, these associations were abrogated by the cell-permeable peptide PRI which is analogous to the first dsRNA binding

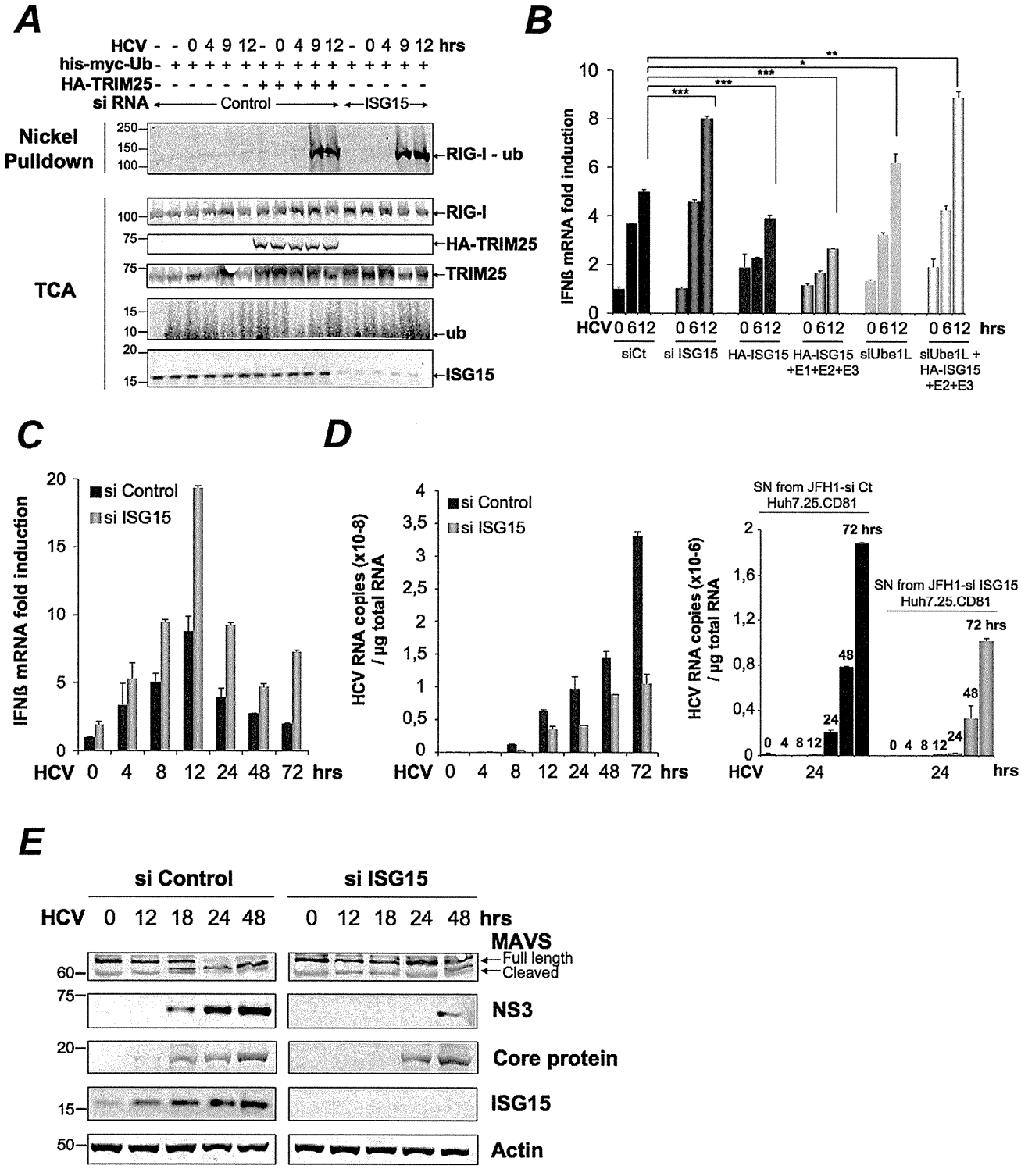

Figure 2. HCV controls RIG-I ubiquitination through ISG15. (**A**) Huh7.25.CD81 cells were transfected for 24 hrs with 25 nM of siRNA (Control or ISG15) and for another 24 hr with 5 µg of a His-Myc-Ubiquitin plasmid in absence or presence of 5 µg of a plasmid expressing HA-TRIM25. The cells were infected with JFH1 (m.o.i = 0.2). At the times indicated, cell extracts were processed for analysis of RIG-I ubiquitination and the expression of the different proteins in the total cell extracts. (**B**) Huh7.25.CD81 cells were first transfected with siRNA Control (25 nM), si RNA ISG15 (25 nM), siRNA Ube1L (50 nM) or left untreated. After 24 hrs, the untreated cells were transfected with a plasmid expressing HA-ISG15 (500 ng) alone or in presence of plasmids expressing E1, E2 and E3 (1 µg each) while a set of cells transfected with siRNA Ube1L received plasmids expressing HA-ISG15, E2 and E3. After 24 hrs, the cells were infected with JFH1 (m.o.i = 6) for the times indicated. Stimulation of endogenous IFNβ RNA expression was determined by RTqPCR and expressed as fold induction. The degree of statistical significance is indicated by stars after calculation of the p-values (from left to right: 0.0005, 0.0076, 0.0003, 0.047 and 0.0023). (**C–D**) Huh7.25.CD81 cells, transfected with 25 nM of siRNA (Control or ISG15) for 48 hrs, were infected with JFH1 (m.o.i = 6) for the times indicated. Expression of IFNβ or HCV RNA, determined by RTqPCR, was expressed as fold induction (**C**; IFNβ) or as copies (**D**; HCV). Error bars represent the mean ±S.D for triplicates. Expression levels of IFNβ RNA at the start of infection were 2.1×10^4 (siControl) and 4×10^4

copies (siISG15). Supernatants collected at different times post-infection were used to infect fresh cells. After 24 hours, the RNAs were extracted from the cells and expression of HCV RNA was determined by RTqPCR. (**E**) Huh7.25.CD81 cells, transfected with 25 nM of siRNA (Control or ISG15) for 48 hrs, were infected with JFH1 for the times indicated. Cell extracts were analysed by immunoblot with Abs directed against ISG15, MAVS, the HCV NS3 and core proteins and Actin as loading control.
doi:10.1371/journal.ppat.1002289.g002

domain (DRBD) of PKR [8], while unaffected by C16, a chemical compound which inhibits the catalytic activity of PKR (**Figure 5D**). In line with this, PRI but not C16, abrogated the ability of HCV to induce ISG15 (**Figure 5E**). The same result was obtained for induction of ISG56 (**Figure S10**). We then used human primary hepatocytes (HHP) to determine whether HCV was also able to induce ISGs through PKR in a more physiological cellular model. A follow-up of the infection over a period of 96 hours showed that JFH1 was replicating correctly in those cells as well as leading to induction of ISG15 (10-fold) and to some induction of IFNβ (2.5-fold). These cells were infected with JFH1 for 8 hours in the absence or presence of PRI, making convenient

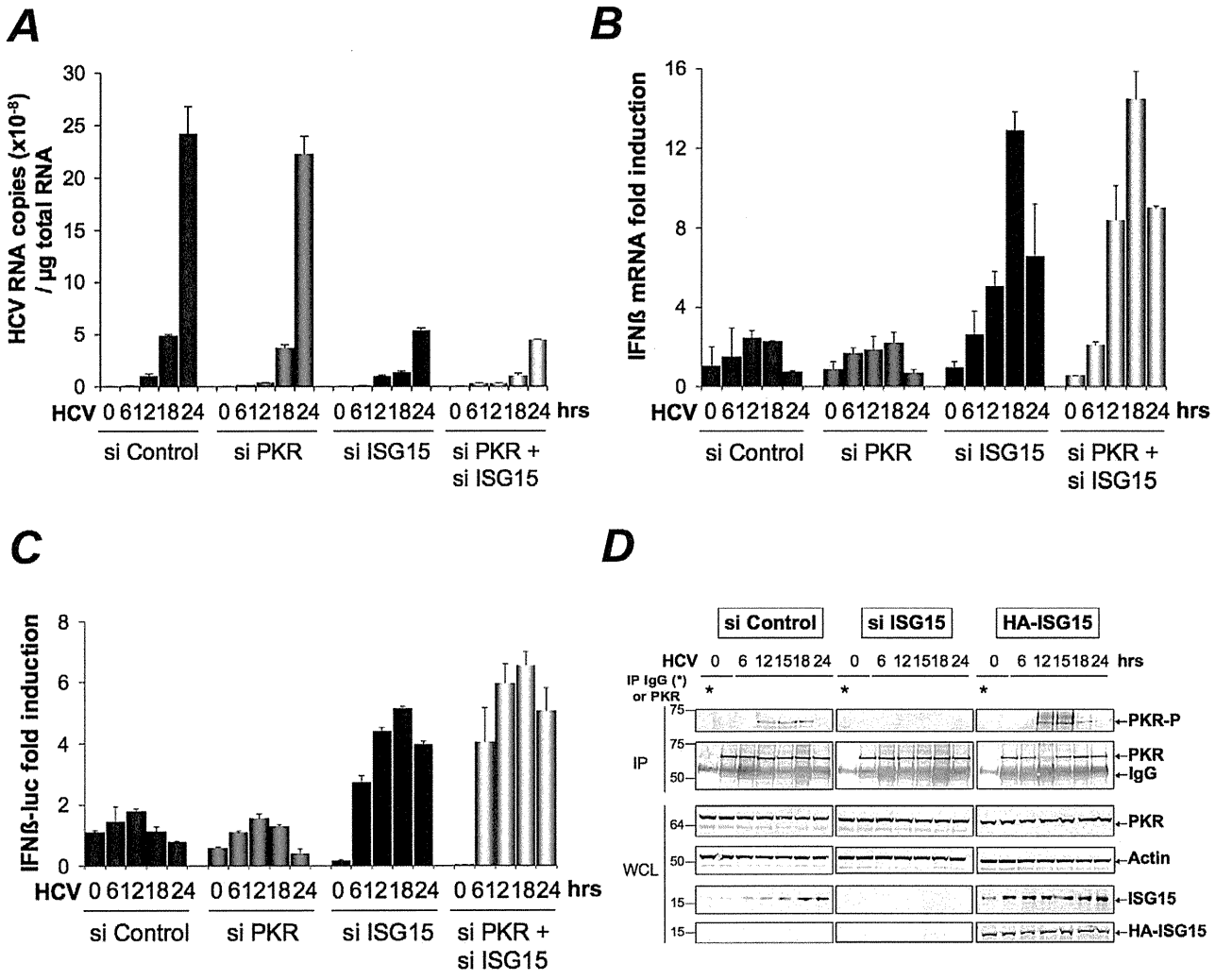

Figure 3. ISG15 strengthens the pro-HCV activity of PKR. (**A–B**). The Huh7.25.CD81 cells were transfected with 25 nM of the different siRNA (Control, ISG15, PKR), separately or together. After 48 hrs, cells were infected with JFH1 (m.o.i = 0.2). At the times indicated, expression of HCV or IFNβ RNA was determined by RTqPCR and expressed as copies of JFH1 RNA (**A**) or as fold induction (IFNβ; **B**). The expression levels of IFNβ RNA at the start of infection was 6.96×10^5 copies. (**C**) Two sets of Huh7.25.CD81 cells were first transfected with siRNA ISG15, siRNA PKR separately and together for 24 hrs, then transfected with the reporter plasmids IFNβ-firefly luciferase (pGL2-IFNβ), pRL-TK Renilla-luciferase for another 24 hrs and infected with JFH1 (m.o.i = 0.2) for the times indicated. In each case, IFN expression was expressed as fold-induction over control cells that were simply transfected with pGL2-IFNβ-FLUC/pRL-TK-RLUC. The graph represents the level of firefly luciferase activity normalized to the ratio R-luc RNA/GAPDH RNA. Such normalization is required because of the negative control of general translation through PKR after 12 hrs post-infection [8]. Error bars represent the mean ±S.D for triplicates. (**D**) Huh7.25.CD81 cells, in 100 cm^2 plates, were transfected with siRNA Control or siRNA ISG15 or transfected with a plasmid expressing HA-ISG15 for 48 hrs and infected with JFH1 (m.o.i = 6). At the indicated times post-infection, cell extracts (2.2 mg) were processed for immunoprecipitation of PKR or for incubation with mouse IgG as a control of specificity (asterisk). The immunoprecipitated complexes were run on two different NuPAGE gels and blotted using Mab 71/10 or anti-phosphorylated PKR antibodies (PKR-P). The presence of PKR and PKR-P was revealed using the Odyssey procedure. The ratio PKR-P/PKR in the absence or in the presence of ISG15, either endogenous or endogenous and ectopic, is shown in Figure S5.
doi:10.1371/journal.ppat.1002289.g003

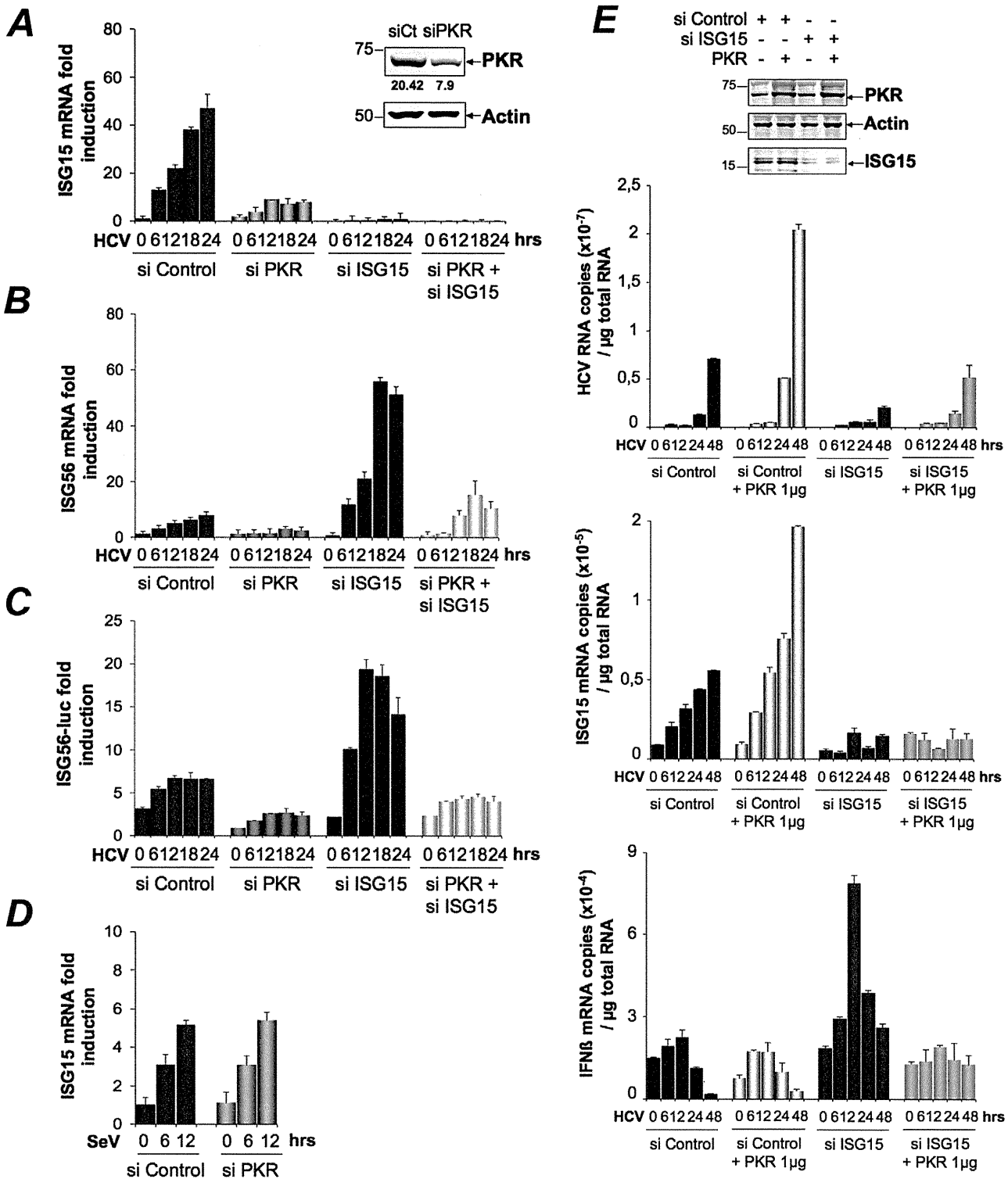

Figure 4. HCV triggers a PKR-dependent pathway early in infection to induce ISG15 and other genes. (**A–C**) The cDNAs reversed transcribed from the RNAs extracted from the Huh7.25.CD81 cells for the experiment described under Figure 3A were analysed by qPCR for the expression of ISG15 (**A**) and ISG56 (**B**). Expression levels of ISG15 and ISG56 RNA at the start of infection were respectively 1×10^5 and 1.18×10^5 copies. A novel set of Huh7.25.CD81 cells were transfected with siRNA Control, siRNA ISG15, siRNA PKR separately and together for 48 hrs. They were then transfected with the reporter plasmids ISG56-FLUC and pRL-TK-RLUC and infected with JFH1 (m.o.i = 0.2). At the times indicated, the effect of the different conditions of silencing on the reporter expression was analyzed after normalization performed as described under Figure 3C (**C**). Results are expressed as fold induction. Error bars represent the mean ±S.D for triplicates. (**D**) Huh7.25.CD81 cells were either transfected with 25 nM of siRNA Control or siPKR for 24 hrs and infected with SeV for the times indicated. Expression of endogenous ISG15 was determined by RTqPCR and expressed as fold induction. Error bars represent the mean ±S.D for triplicates. The expression levels of ISG15 RNA at the start of infection were respectively 4.91×10^4 copies (siControl) and 5.44×10^4 copies (siPKR). (**E**) Huh7.25.CD81 cells were either transfected with 25 nM of siRNA Control or

siISG15 and with 1 μg of a plasmid expressing PKR where indicated. After 48 hrs, the cells were infected with HCV (m.o.i = 6) for the times indicated. Expression of HCV, ISG15 and IFNβ RNA was determined by RTqPCR. Cell lysates prepared from cells treated in the same conditions but not infected were used to control expression of PKR and ISG15 by immunoblot.
doi:10.1371/journal.ppat.1002289.g004

use of the cell-penetrating ability of this peptide. Longer period of treatment with PRI were not investigated for practical reasons (see Materials and Methods). The results showed that PRI was significantly inhibiting the induction of ISG15 while it had no effect on that of IFNβ (**Figure 5F**). Altogether, these data demonstrate that HCV triggers induction of early ISGs through MAVS and TRAF3 by using PKR as an adapter protein.

PKR interacts both with MAVS and TRAF3 and binds HCV RNA ahead of RIG-I

The ability of HCV to control activation of the RIG-I/MAVS pathway after induction of ISG15 through a novel PKR/MAVS pathway suggests that PKR has the possibility to bind MAVS prior to RIG-I. To determine this, we established the kinetics of these interactions, after treating the Huh7.25.CD81 cells with siRNAs targeting ISG15 prior to HCV infection. This was necessary in view of the negative control of ISG15 on RIG-I. MAVS was immunoprecipitated from the cell extracts at different times post-infection and the presence of PKR and RIG-I was examined in the immunocomplexes, as well as that of TRAF3, used as marker of activation of the MAVS signaling pathway. As expected, only PKR was able to associate with MAVS and TRAF3 in the control cells (**Figure 6A**) whereas both PKR, RIG-I and TRAF3 were found in the immunocomplexes in the absence of ISG15 (**Figure 6B**). The PKR/MAVS association took place at 4 hrs post-infection in the control cells but was observed 2 hrs earlier in the ISG15-depleted cells. Whether ISG15 plays a role in the regulation of the PKR/MAVS association remains to be determined. However, the presence of TRAF3 in association with MAVS at 2 hrs post-infection in the control cells (**Figure 6A**) correlates with its association with PKR (**Figure 5C**) which indicates that the MAVS pathway can be activated through PKR as soon as 2 hrs post infection. In ISG15 knock-down cells, the RIG-I/MAVS association occurred later at 6 hrs post-infection with an increase in TRAF3 association at 9–12 hrs post infection. Altogether, these data revealed that HCV infection triggers an earlier interaction of MAVS with PKR than with RIG-I.

Finally, we asked whether PKR was able to associate with HCV RNA and how this association can be compared to that of RIG-I. PKR and RIG-I were immunoprecipitated at 2, 4 and 6 hrs post-infection and the presence of HCV RNA was analysed in the complexes. The results showed that PKR associates with HCV RNA with best efficiency at 2 hrs post-infection. Importantly, this association was strongly inhibited in presence of PRI, thus confirming the importance of PKR DRBD in the process. In contrast, the association of HCV RNA with RIG-I was detected only at 6 hrs post-infection. Interestingly, the association between RIG-I and HCV RNA was not affected by PRI, which rules out the possibility that the initial formation of a complex between PKR and HCV RNA was a pre-requisite for the subsequent binding of RIG-I to HCV RNA. Immunoprecipitation of PKR at 1, 2, 4 and 6 hrs post-infection, in presence of an inhibitor of ribonucleases also did not lead to detection of RIG-I in the complexes (**Figure S11**). Association of HCV RNA with eIF2α, used as negative control, was not significant, thus showing the specificity of the assay (**Figure 6C**). Whether a direct interaction of PKR with HCV RNA represents the initial event leading to the MAVS-dependent induction of early ISGs remains now to be characterized. Altogether, these data reveal an earlier mobilization of PKR than RIG-I in response to HCV infection which leads to activation of a MAVS-dependent signaling pathway.

Discussion

Hepatitis C virus can attenuate IFN induction at multiple levels in infected hepatocytes, such as through the NS3/4A-mediated MAVS cleavage [7,27] and by using the eIF2α kinase PKR to control IFN and ISG expression at the translational level [8,9]. Here, we have identified another process by which HCV controls IFN induction at the level of RIG-I ubiquitination through ISG15 and an ISGylation process. Importantly, we have shown that ISG15 is rapidly induced, among other ISGs, in response to HCV infection, through a novel signaling pathway that involves PKR, MAVS, TRAF3 and IRF3 but not RIG-I. In this pathway, PKR is not used for its kinase function but rather as an adapter protein with its dsRNA binding domain (DRBD) playing an essential role in this mechanism (**Figure 7**). By transcriptome analysis, we showed that HCV induces a number of ISGs in the HCV-permissive Huh7.25.CD81 cells and we confirmed the induction of two of these, ISG15 and ISG56, in other HCV-permissive cells, such as Huh7.5 and Huh7 cells. In addition, induction of ISG15 by HCV in a PKR-dependent manner was confirmed in human primary hepatocytes. The ability of HCV to trigger high expression levels of ISG15 and ISG56, as well as other ISGs, has previously been reported in models of HCV-infected chimpanzees [10,12,28] and in HCV-infected patients [14,15,16]. Induction of ISGs thus represents a general propriety of the response of the cells to HCV. In addition to this, natural variations in intra-hepatic levels of ISG15 *in vivo* may increase the susceptibility of some patients to HCV infection. The ability of HCV to control RIG-I activity through ISG15 is important to note in view of several reports which highlight the importance of a role for ISG15 in the maintenance of HCV in livers [15,16] or in the control of HCV replication in cell cultures [17,25]. Our data provide an explanation for the presence of ISGs at high expression levels in HCV-infected patients [14,15,16] and in models of HCV-infected chimpanzees [10,12,28] in the absence of, or with poor IFN expression.

The 15 Kda ISG15, or Interferon Stimulated Gene 15 [29], also known as ubiquitin cross reactive protein (UCRP) [30], can be conjugated (ISGylation) to more than 150 cellular protein targets [31] through the coordinated action of three E1, E2 and E3-conjugating enzymes, in a process similar but not identical to ubiquitination. While both ubiquitin and ISG15 can use the same E2 enzyme UbcH8, Ube1L functions as a specific E1 enzyme for ISG15, in spite of its 45% identity with Ube1, the E1 enzyme for ubiquitin [32]. The major E3 ligase for human ISG15 is HERC5 [33].

Interestingly, RIG-I was identified as a target for ISG15, among other IFN-induced proteins or proteins involved in IFN action [31]. However, its activity appears to be negatively controlled by ISG15 and the ISGylation process, either as shown previously after cotransfection with the ISG15 and the ISG15-conjugating enzymes [18] or as shown here, in a model of infection with HCV. Indeed, ISG15 is now emerging as playing a proviral role in case of HCV infection. Several reports now highlight the importance of a role for ISG15 in the control of HCV replication in cell cultures [17,25] as well as in the maintenance of HCV in livers and

Table 1. PKR-dependent up-regulated genes upon HCV infection.

SiPKR mock/siCt	Name	Access. N.	siCtMock	siCt HCV	siCtMock'	siPKRHCV	LOG2*
0,6	**ISG56**	NM_001548	15,0	885,8	10,2	7,6	-6,3
0,7	**ISG15**	NM_005101	593,6	26061,9	410,6	283,5	-6,0
0,7	**IFI 9-27/IFITM1**	NM_003641	27,8	817,7	15,1	10,1	-5,5
1,2	**IFI1-8U**	NM_006435	24,0	597,7	10,9	7,2	-5,3
1,1	Olfactory Receptor 9I1	NM_001005211	26,6	473,1	10,1	4,8	-5,2
1,6	IFI1-8U	XM_084845	17,7	365,4	9,3	6,5	-4,9
0,8	**OASp100**	NM_006187	46,4	909,9	40,0	33,5	-4,5
0,8	**IFI6-16**	NM_002038	834,5	10040,6	45,9	24,1	-4,5
0,6	**Ub2L6**	NM_004223	392,7	4078,9	281,2	128,7	-4,5
0,9	**OAS 1**	NM_016816	49,9	704,03	31,8	21,6	-4,4
0,9	**ISG12**	NM_005532	46,3	592,54	38,3	29,2	-4,1
0,8	**IFP 35**	NM_005533	36,3	369,7	26,6	16,9	-4,0
0,6	PARP-9	NM_031458	29,5	318,5	37,8	25,6	-4,0
0,5	GABA-B receptor 1	NM_006398	29,5	500,8	26,0	28,5	-4,0
0,7	**Lysp100B**	NM_003113	8,7	93	8,5	6,1	-3,9
0,8	PDIP1	NM_033405	27,4	146,6	28,0	12,8	-3,6
0,8	**PKR**	NM_002759	48,2	306,8	47,0	26,0	-3,5
1,6	**MT-IM**	NM_176870	49,0	1371,8	6,9	19,6	-3,3
0,7	**Phospholipid scramblase**	NM_021105	170	1137,2	189,9	153	-3,1
1,1	**RIG-I**	NM_014314	23,5	223,2	18,9	21,9	-3,0
0,6	**IFIT-5**	NM_012420	24,9	95,3	35,0	21,3	-2,7
1,3	RIG-I	NM_004585	7,4	42,5	6,3	6,0	-2,6
0,7	**STAT1 beta**	NM_139266	336,9	1401,5	300,3	210,3	-2,6
0,8	BRCA1 C-ter assoc. Prot	NM_001040444	12,3	45,1	8,1	5,1	-2,6
0,9	Cohesin Rec8 homolog	NM_005132	18,0	103	16,7	16,9	-2,5
0,5	C/EBPdelta	NM_005195	324,9	901,8	278,9	161,27	-2,3
0,7	ZNF532	NM_018181	32,8	146,5	25,5	23,8	-2,3
0,6	NNMT	NM_006169	52,8	143,8	50,26	28,9	-2,2
1	ISG1-8U	XM_084845	32,0	146,8	23,1	22,7	-2,2
1,1	HIF00	NM_153833	45,3	199,9	34,7	32,9	-2,2
0,8	**ISG20**	NM_002201	129,3	338,3	107,5	61,4	-2,2
1,1	PSMB10	NM_002801	16,2	75,1	14,5	15,0	-2,2
1,3	ZC3HAV1	NM_024625	8,3	26,0	6,9	4,9	-2,1
0,9	SOD2	NM_000636	348,5	1612,2	311	334,3	-2,1
0,7	PARP12	NM_022750	269,9	875,2	296,9	224,2	-2,1
0,7	NMI	NM_004688	32,1	136	37,4	37,0	-2,1
0,8	NEDD9	NM_006403	5,7	19,0	5,7	4,7	-2,0
1,1	**SAMHD1**	NM_015474	17,1	49,5	13,6	9,7	-2,0
0,7	AKT2	NM_001626	13,4	20,0	14,2	5,4	-2,0
0,5	ARG1	NM_000045	245,9	282,6	231,4	67,0	-2,0
0,8	BHLHB2	NM_003670	76,4	128,0	71,5	30,5	-2,0
0,8	LGALS3BP	NM_005567	22,0	72,0	16,1	13,6	-2,0
1,3	ZNF292	XM_048070	22,3	31,4	20,2	7,3	-2,0
1,1	STAT1	NM_007315	53,3	275,3	48,2	64,9	-1,9
0,7	TBA3_HUMAN	NM_006009	28,2	43,6	33,4	13,7	-1,9
0,5	TM4SF20	NM_024795	45,2	51,0	36,9	11,1	-1,9
1,4	ERAP2	NM_022350	9,8	19,2	8,8	4,6	-1,9
0,8	**USP18**	XM_001126794.1	215,1	979,2	201,8	245,9	-1,9
1	USP18	XM_001126794.1	129,6	617,0	127,3	165,5	-1,9